Contrasting local climate velocity impacts in warm and cool locations: a meta-analysis across 38 demersal fish species in the northeast Pacific

Philina A. English[1,*], Eric J. Ward[4], Christopher N. Rooper[1], Robyn E. Forrest[1], Luke A. Rogers[1], Karen L. Hunter[1], Andrew M. Edwards[1,3], Brendan M. Connors[2], and Sean C. Anderson[1,5]

[1]Pacific Biological Station, Fisheries and Oceans Canada, Nanaimo, BC, Canada
[2]Institute of Ocean Sciences, Fisheries and Oceans Canada, Sidney, BC, Canada
[3]Department of Biology, University of Victoria, Victoria, BC, Canada
[4]Northwest Fisheries Science Centre, National Marine Fisheries Service, National Oceanographic and Atmospheric Administration, Seattle, WA, USA
[5]Department of Mathematics, Simon Fraser University, Burnaby, BC, Canada
[*]corresponding author: philina.english@dfo-mpo.gc.ca

Abstract

Species responses to climate change are often measured at broad spatiotemporal scales; however, doing so can miss fine-scale changes that may take place more quickly and be more directly relevant to local conservation and fisheries management decisions. Here, we develop a fine-scale geostatistical approach to assess how fish distributions have been shaped by local changes in temperature and dissolved oxygen over a recent decade of warming in the northeast Pacific. We estimate distribution change by maturity class (juvenile, mature) for 38 demersal fish species using spatiotemporal models that allow depth preferences to vary. Across species, biomass trends were associated negatively with warming and positively with dissolved oxygen. In contrast, when trends in both biomass and climate were converted to velocities—the speed and direction an organism would have to move to maintain consistent conditions—the effect of temperature change differed depending on local conditions. In the warmest locations, warming velocities were associated with negative biotic velocities for 19 of 69 species-maturity combinations, and yet were almost always associated with stable or positive biotic velocities in the coolest locations (64 of 69). After accounting for the effect of temperature, dissolved oxygen velocities were associated with biotic velocities for ~34% of species. However, this relationship was negative more often than positive, which suggests a mechanism other than hypoxia avoidance—possibly changes in primary production. We also examined relationships between these effects and each species' ecology, but did not find any strong relationships. Evidence of spatially consistent biomass declines (negative biotic velocity) in the warmest locations and increases in cooler locations suggests a redistribution of species with the potential for new ecological and fisheries interactions. Our approach identifies which species and locations are likely to be most vulnerable to these changes using methods that are flexible across scales relevant to conservation and fisheries management.

Introduction

Managing the impacts of a rapidly changing climate on ecological communities, particularly those that provide food for humans, is a critical challenge facing society (e.g., Doney *et al.* 2012). An increase in atmospheric CO2 is not only causing increases in both mean ocean temperature and the frequency of extreme heat waves (Frölicher *et al.* 2018), but is also affecting patterns of circulation, productivity, and marine chemistry (Pörtner *et al.* 2019). Combined, these environmental changes can impact the distribution and abundance of many ecologically and commercially important fish species, leading to local loss of some species, colonizations, and changes in species interactions and bycatch composition (e.g., Pinsky and Fogarty 2012, García Molinos *et al.* 2016, Morley *et al.* 2018). Furthermore, such changes can lead to temporary climate-induced hyperstability—catch rates that remain high despite population declines—if organisms move towards preferred habitat during population decline, or if population density increases faster than range expansion during population growth (the basin model of density-dependent habitat selection theory; MacCall 1990, Thorson *et al.* 2016b). Because traditional stock assessment methods, fisheries regulations, and choices regarding habitat protection generally assume stationary species distributions, new methods that anticipate and incorporate the effects of climate change on species distributions will be crucial for successful resource management in the future (Hare *et al.* 2010, Bell *et al.* 2020).

Species responses to climate change are often studied along range edges (Parmesan and Yohe 2003, Sunday *et al.* 2015, Fredston *et al.* 2020, Fredston-Hermann *et al.* 2020) or as aggregate indices (e.g., at species or region levels; Pinsky *et al.* 2013, Thorson *et al.* 2016a, Morley *et al.* 2018). The centre of gravity is perhaps the most commonly used measure of changes in distribution for marine fishes (e.g., Perry *et al.* 2005, Rindorf and Lewy 2006, Dulvy *et al.* 2008, Nye *et al.* 2009, Adams *et al.* 2018, Rooper *et al.* 2020). However, these approaches can overlook fine-scale spatial variation that may be important for understanding species responses (Oldfather *et al.* 2020) and distribution shifts may take longer to manifest at aggregate scales. Aggregate measures such as the centre of gravity are also challenging to interpret and apply in cases where both surveys and management actions are constrained by geographic or political boundaries that partition the distribution of a species. Indeed, laboratory experiments have demonstrated that thermal tolerances and optimums can differ sub-regionally (e.g., Pörtner *et al.* 2008) and there is evidence that warm range edges have shifted further north than expected and cold range edges contracted southward (in the northern hemisphere), which suggest roles for competition, depredation, and/or density dependent habitat selection (Fredston *et al.* 2020). Despite this, projections of future species' distributions often assume that responses to climate variables are consistent across space and time (e.g., Morley *et al.* 2018). While coarse-scale changes can be informative for long-term planning, changes in local abundances at finer spatial scales will likely occur more quickly due to the shorter dispersal distances involved and may be more informative in steering local conservation actions.

Local velocities are commonly used to quantify changes at finer spatial scales than captured in population-wide indices (e.g., Brito-Morales *et al.* 2018). A local climate velocity represents the movement of an isocline—a boundary along which a climate metric is constant. More intuitively, a climate velocity gives the speed and direction an individual must move to maintain a constant

climate condition (e.g., temperature) (Loarie *et al.* 2009). Gradient-based estimates of climate velocity are calculated as a trend in a climate metric through time (e.g., temperature trend), which can be positive or negative, divided by the local gradient in space comprised of a magnitude and direction (see Methods Eq. 12; Table 1; Burrows *et al.* 2011). These velocities scale local climate trends to emphasize locations where climate is relatively consistent across a neighbourhood of cells. Alternatively, analog-based velocities are estimated using search algorithms that identify nearest climate matches within a user-defined threshold of change from the reference cell conditions (Hamann *et al.* 2015). While analog-based velocity estimates can be more geographically precise, the choice of thresholds and other statistical properties (e.g., clumpiness) make them less useful than gradient-based local velocities for meta-analysis (Ordonez and Williams 2013).

Changes in abundance, density, or probability of species occurrence can also be expressed as velocities (e.g, Serra-Diaz *et al.* 2014, Comte and Grenouillet 2015, Alabia *et al.* 2018). When applied to species distribution models, these are referred to as biotic velocities and can be thought of as the minimum distance one would have to move to maintain an equivalent degree of habitat suitability (Carroll *et al.* 2015, Comte and Grenouillet 2015). Similarly to climate velocity, a positive local biotic velocity is associated with an increase in habitat suitability at the focal location and a negative value represents a decline in suitability. The magnitude of the velocity estimates the distance to the nearest location that is predicted to match the original probability of occurrence or abundance. Because changes in climate may cause shifts in fish population density before range shifts based on presence-absence are clearly detectable, abundance and biomass-based models of species distributions are potentially more sensitive to local change than simple occupancy estimates.

Bottom-trawl fisheries tend to capture a taxonomically and ecologically diverse suite of fishes. For example, the groundfish bottom-trawl fishery in Canadian Pacific waters encounters >100 species (Anderson *et al.* 2019), many of which are managed via an individual transferable quota system with 100% at-sea and dockside monitoring (Turris 2000, Wallace *et al.* 2015, DFO 2019). Random depth-stratified fishery-independent bottom trawl surveys have been fitted with conductivity, temperature, depth (CTD), and dissolved oxygen (DO) sensors since 2008. In addition to estimates of biomass density for each species captured in the surveys, data on size distributions and reproductive maturity are collected for many species (Anderson *et al.* 2019). Collectively, these species occupy a large range of depths, especially along the shelf edge where short movements can result in large environmental changes, and vary in their potential for behavioural responses to climate. For example, some species are migratory or highly mobile (e.g., Sablefish, *Anoplopoma fimbria*, many flatfish species), while others are relatively sedentary (e.g., many species of rockfish, *Sebastes* spp.).

Here, we explore the extent to which groundfish distributions in the northeast Pacific have been shaped by local temperature and DO trends and velocities over a decade spanning a relatively cool period through a recent marine heat wave (Okey *et al.* 2014, Frölicher and Laufkötter 2018). We do this by quantifying broad patterns and species-level relationships between climatic and biotic change in order to answer the following questions: (1) Are local changes in bottom temperature or DO correlated with changes in local groundfish densities, and are these effects stronger in already warm or low-oxygen regions? For example, has local warming had a larger

effect in locations that are already at the warm-extreme of a species' local distribution? (2) How do these relationships differ between the spatial contexts captured by gradient-based velocities vs. their component trends? (3) How do these effects vary between species and are they correlated with life-history characteristics such as age and growth rate; or ecological traits such as depth range, latitude, trophic level, foraging zone, or sociality? We address these questions by using spatiotemporal models applied to a decade of survey-derived climate and species density data, and then assess relationships between velocities of biotic and climatic change for 38 commonly encountered species using a geostatistically explicit hierarchical analysis that controls for change in both temperature and DO.

Methods

Survey data

We analyzed biomass density distributions and morphometric data for 38 species of groundfish that were regularly encountered by fisheries-independent bottom-trawl surveys and are widely distributed within Canadian Pacific waters (Table S1). The surveys were stratified within four regions, two of which were surveyed in odd years (Hecate Strait and Queen Charlotte Sound) and two in even years (West Coast Vancouver Island and West Coast Haida Gwaii) since at least 2005. Each region was sampled over the same month-long period between late May and early August in each survey year. Combined, these surveys covered most of the upper continental slope and shelf in Pacific Canada and shared similar random depth-stratified designs, fishing gear, and fishing protocols (Sinclair *et al.* 2003). We only included tows of $>$ 15 minutes duration and converted total biomass of each species to a biomass density based on the speed, distance covered, and net opening (e.g., Williams *et al.* 2018, Anderson *et al.* 2019). Biological sampling protocols varied among species, depending on size of catch and commercial importance. In general, catches of between 10–50 fish were sexed, weighed and measured individually, while larger catches were subsampled and, for commercially important species, data on maturity and otoliths for aging were collected.

Estimating spatiotemporal variation in maturity-specific fish biomass density

Because ontogenetic shifts in habitat, particularly depth, are well documented for groundfish species (e.g., Mindel *et al.* 2016, Barbeaux and Hollowed 2018, Li *et al.* 2019), we estimated biomass densities separately for mature and immature size classes whenever possible. Maturity was not assessed for certain Chondrichthyans, or when catches were particularly low. To do this, we first estimated length at 50% maturity as defined by gonadal development stages using ogives fit as sex-specific logistic regressions to individual specimens (see Supplementary Methods). To split the estimated biomass density per tow into mature and immature components, we calculated the summed biomass of all measured fish that were above (for mature) or below (for immature) the length-at-50% maturity threshold, divided by the total biomass of all measured fish, and multiplied this ratio by the estimated biomass density for each tow. For each tow that resulted in too small

a catch for detailed measurements to have been taken, we applied the mean ratio from all measured tows to estimate mature biomass (applied to a median of 9% [range 1–40%] of each species' total sampled biomass). For species without any maturity data, we assumed that the total biomass estimate represented the mature population, because mature individuals are larger, and therefore likely to be numerically dominant (* in Table S1). However, it is possible that biomass sampled in some areas was actually dominated by immature individuals, particularly for the skate species, whose mean lengths fall close to the sizes at maturity found in Love (2011).

We modelled spatiotemporal biomass density separately for mature and immature fish of each species using spatial GLMMs. Environmental variables, such as temperature, may be included in these models explicitly and can be used to assess the vulnerability or tolerance of a given species to change (Godefroid *et al.* 2019). However, such approaches require strong assumptions (e.g., that effects are constant through both time and space). Instead, we use a climate-agnostic version of a species distribution model with a spatiotemporal random effect structure to estimate local variability in biomass density change. Our models relied on spatial random effects to capture unmeasured components of habitat suitability and allow suitability to change through time without making assumptions about the shape of species-specific responses to possible climatic and geographic covariates (e.g., Shelton *et al.* 2014, Ward *et al.* 2015, Thorson *et al.* 2015b, 2017). We modelled each species and maturity class separately because, although these density patterns are correlated, explicitly modelling those relationships among groundfish species has not been shown to dramatically improve precision of overall estimates (Thorson and Barnett 2017), and maintaining independent estimates should make identification of shared climate responses more conservative.

We modelled biomass density with a Tweedie distribution and a log link because densities contain both zeros and positive continuous values (Tweedie 1984, Dunn and Smyth 2005, Anderson *et al.* 2019):

$$Y_{s,t} \sim \text{Tweedie}\left(\mu_{s,t}, p, \phi\right), \; 1 < p < 2, \tag{1}$$

$$\mu_{s,t} = \exp\left(\alpha_t + \gamma_{1,t} D_{s,t} + \gamma_{2,t} D_{s,t}^2 + \omega_s + \epsilon_{s,t}\right), \tag{2}$$

$$\gamma_{1,t} \sim \text{Normal}\left(\gamma_{1,t-1}, \sigma_{\gamma_1}^2\right), \tag{3}$$

$$\gamma_{2,t} \sim \text{Normal}\left(\gamma_{2,t-1}, \sigma_{\gamma_2}^2\right), \tag{4}$$

$$\boldsymbol{\omega} \sim \text{MVNormal}\left(\mathbf{0}, \boldsymbol{\Sigma}_{\omega}\right), \tag{5}$$

$$\boldsymbol{\epsilon}_t \sim \text{MVNormal}\left(\mathbf{0}, \boldsymbol{\Sigma}_{\epsilon}\right), \tag{6}$$

where $Y_{s,t}$ represents the biomass density at point in space s and time t, μ represents the mean biomass density, p represents the Tweedie power parameter, and ϕ represents the Tweedie dispersion parameter. The parameter α_t represents the mean effect for each year, and $\gamma_{1,t}$ and $\gamma_{2,t}$ represent time-varying coefficients associated with depth (D) and depth-squared covariates (D^2), respectively, which both follow a random walk constrained by $\sigma_{\gamma_1}^2$ and $\sigma_{\gamma_2}^2$. The initial values $\gamma_{1,t}$ and $\gamma_{2,t}$ at $t = 1$ share an implied Uniform$(-\infty, \infty)$ prior. We considered alternative covariates not described here (Supporting Methods) The parameters ω_s and $\epsilon_{s,t}$ represent spatial and spatiotem-

poral random effects that were assumed drawn from Gaussian Markov random fields (e.g., Latimer *et al.* 2009, Cressie and Wikle 2011, Lindgren *et al.* 2011) with covariance matrices Σ_ω and Σ_ϵ that were constrained by Matérn covariance functions (Cressie and Wikle 2011). The covariance matrices for a given maturity-species combination shared a common κ parameter that controls the rate of decay of spatial correlation with distance (Cressie and Wikle 2011).

We modelled the spatial components as random fields using a triangulated mesh with vertices selected using a k-means algorithm (via the k-means function in R; e.g., Shelton *et al.* 2014) at a specified number of locations, known as knots, used to approximate the spatial variability in observations. We used 500 knots for mature density, 400 for immature density, and 300 for less well-sampled species (Bocaccio *Sebastes paucispinis*, Shortraker *Sebastes borealis*, and immature Redstripe Rockfish *Sebastes proriger*). Based on estimated values of the spatial surface at these knot locations, we used bilinear interpolation to approximate a continuous spatial field (Rue *et al.* 2009, Lindgren *et al.* 2011).

We fit our models in R version 3.6.1 (R Core Team 2019) with the R package `sdmTMB` (Anderson *et al.* 2019, 2020), which interfaces automatic differentiation and the Laplace approximation in the `TMB` (Template Model Builder) R package (Kristensen *et al.* 2016) with the SPDE (Stochastic Partial Differential Equation) approximation to Gaussian Markov fields from the `INLA` (Integrated Nested Laplace Approximation) R package (Rue *et al.* 2009) to find the value of the fixed effects that minimizes the the marginal negative log likelihood. We confirmed that the non-linear optimizer had converged by checking that the Hessian matrix was positive definite and the maximum absolute gradient across fixed effects was < 0.005.

Estimating climate velocities

Bottom temperature and dissolved oxygen (DO) levels have been collected on most tows during the synoptic bottom trawl surveys since 2008, using Seabird Electronics SBE 19 profilers. From these measurements, we predicted seafloor climate using an approach similar to the one described above for biomass density except we used a Gaussian observation model, 800 knots, and allowed the spatiotemporal random fields to follow an autoregressive (AR1) process:

$$C_{s,t} \sim \text{Normal}\left(\mu_{s,t}, \sigma^2\right), \tag{7}$$

$$\mu_{s,t} = \boldsymbol{X}_{s,t}\boldsymbol{\beta} + \omega_s + x_{s,t}, \tag{8}$$

$$\boldsymbol{\omega} \sim \text{MVNormal}\left(\mathbf{0}, \Sigma_\omega\right), \tag{9}$$

$$\boldsymbol{x}_{t=1} \sim \text{MVNormal}(\mathbf{0}, \Sigma_\epsilon), \tag{10}$$

$$\boldsymbol{x}_{t>1} = \rho\boldsymbol{x}_{t-1} + \sqrt{1-\rho^2}\boldsymbol{\epsilon}_t,\ \boldsymbol{\epsilon_t} \sim \text{MVNormal}\left(\mathbf{0}, \Sigma_\epsilon\right). \tag{11}$$

Here $C_{s,t}$ represents the climate variable (bottom temperature or log DO) in space s and time t, μ represents the mean, and σ represents the observation error standard deviation. The symbol $\boldsymbol{X}_{s,t}$ represents a vector of predictors (described below) and $\boldsymbol{\beta}$ represents a vector of corresponding parameters. The spatial random effects ω_s were defined as in Eq. 5 whereas the spatiotemporal random effects were structured to follow a stationary AR1 process with first-order correlation

ρ. Because DO is known to be influenced by both water temperature and seasonal biological processes, we included a quadratic effect for temperature and a linear effect for day of year along with estimated means for each year. Although not shown above for simplicity, we again allowed the quadratic depth covariates to follow a random walk through time as in Eq. 3. Our bottom temperature model fixed effects included only estimated means for each year (and depth effects), because inclusion of day of year did not improve model fit based on AIC (Akaike Information Criterion). Because bottom temperature data (but not DO) have been collected in synoptic surveys since 2003, we included these earlier data in the temperature model to provide more information for estimating the fixed spatial random field and depth effects ω_s.

For all climate and biomass models, we then projected the model predictions onto a 4×4 km grid (UTM 9 projection) representing the survey domain. We excluded all cells with predicted conditions outside the range of conditions observed during sampling (99% quantiles of 3.07 to 11.3 °C and 0.28 to 7.06 ml/L DO). We then calculated gradient-based velocities of change and constituent local trends and spatial gradients for each cell. Gradient velocities (V) were calculated as a ratio of the temporal trend (linear regression slope of each cell's climate time series) divided by gradient in space g of variable A

$$V_s = (\Delta A_s / \Delta t) \, / g_s, \tag{12}$$

where A is any temporally varying feature of focal cell s. Depending on the portion of the survey grid considered, we calculated the trend through time for biennial time-steps between 2008 and 2018 (6 surveys across 10 years) or 2009 and 2017 (5 surveys across 8 years), but reported values for all cells as a rate of change, or trend, per decade (Table 1). The spatial gradient g_s was calculated as the vector sum of the mean north-south and east-west gradients based on a $3x3$ cell neighbourhood (Burrows *et al.* 2011); however, the values of A from which a spatial gradient is calculated can be based on any particular subset of times t, or the mean of all Δt.

The magnitudes of gradients g_s strongly influence the distribution of velocities V. Most prior applications of gradient-based velocities have used g_s calculated from the mean cell conditions of the entire period analyzed (e.g., Burrows *et al.* 2011, Molinos *et al.* 2019). Estimated velocities will tend to be larger (as $g_s \to 0, V_s \to \infty$) when more estimates (in this case sample years) are averaged for the cells included in the g_s calculation, because a larger sample reduces the variability between the mean values of adjacent cells. Furthermore, the gradients most relevant to the actual distance an organism would need to travel are those present after changes have begun to occur. Given that samples were collected only once every two years and that there is variability among species in terms of when dispersal occurs and how long it takes, we used the last two sample periods in our estimates of spatial gradients (2015–2018). This time period begins the first survey season following the onset of the 2014–2016 marine heat wave in the north-eastern Pacific (Peterson *et al.* 2015) and is approximately the end point of the transition to warmer conditions in the Bering sea (Alabia *et al.* 2018). We calculated spatial gradients using the `vocc` R package (Brown and Schoeman 2020) and collapsed extreme velocity estimates to their 0.005 and 0.995 quantiles to reduce the impact of outliers from the resulting heavy-tailed distributions.

Linking biotic changes with climate

To explore the relationship between change in estimated local climate and percent changes in estimated biomass densities for each 4×4 km grid cell, we used similar spatial GLMMs to control for spatial autocorrelation among cells. Our models estimated the rate of change in biomass (Y) of each maturity class of each species as a function of local climate change (temperature and DO) and an interaction between the mean climate of each cell and its local rate of change:

$$\Delta Y_{k[s]} \sim \text{Normal}\left(\mu_{k[s]}, \sigma^2\right), \tag{13}$$

$$\begin{aligned}\mu_{k[s]} = {} & \beta_{0,k[s]} + \beta_{1,k[s]}\overline{T}_s + \beta_{2,k[s]}\Delta T_s + \beta_{3,k[s]}\overline{T}_s\Delta T_s + \\ & \beta_{4,k[s]}\overline{O}_s + \beta_{5,k[s]}\Delta O_s + \beta_{6,k[s]}\overline{O}_s\Delta O_s + \beta_{7,k[s]}\overline{Y}_{k[s]} + \omega_{k[s]},\end{aligned} \tag{14}$$

$$\boldsymbol{\omega}_k \sim \text{MVNormal}\left(\mathbf{0}, \boldsymbol{\Sigma}_\omega\right), \text{ for } k = 1, \ldots, K, \tag{15}$$

$$\beta_{r,k} \sim \text{Normal}\left(\eta_{r,k}, \sigma^2_{\beta_r}\right), \text{ for } k = 1, \ldots, K \text{ and } r = 0, \ldots, 7, \tag{16}$$

where $\overline{T}_s$ and ΔT_s represent the mean temperature and decadal trend in temperature for spatial location s. A row of data represents a given spatial grid cell s and species-maturity k combination. The symbols $\overline{O}_s$ and ΔO_s represent mean dissolved oxygen and decadal trend in dissolved oxygen, and the symbol $\overline{Y}_{k[s]}$ represents log biomass density for species-maturity k. Parameters β_0 through β_7 (indexed by r) represent coefficients that are allowed to vary as random effects across species with means $\eta_{r,k}$ and variances $\sigma^2_{\beta_r}$. We accounted for spatial autocorrelation through the spatial random effects $\omega_{k[s]}$, which follow a Matérn Gaussian Markov random field as described above.

We fit model configurations where both biomass and climate were calculated as either raw temporal trends or gradient-based velocities. The trend-based models assessed whether biomass changes were correlated with changes in climate at the 4×4 km grid cell scale. The velocity-based models assessed whether changes in biomass, especially those with low local variability in biomass, were correlated with the predicted speed of climate isoclines within the 12×12 km neighbourhood of cells. We did not include both trends and velocities in the same model because both the units and spatial scales captured are different.

For each maturity class of each species, we included all grid cells that encompassed 95% of the mean total biomass across all sample years and the mean log biomass density of each cell as a covariate to reduce the influence of changes occurring only at either the highest or lowest densities for a particular species. These models used a 600 knot mesh, Gaussian observation errors when estimating trends, and Student-t observation errors (with a degrees of freedom fixed at 7) to account for heavy-tailed residuals when estimating velocities. We scaled all covariates by their standard deviations. We centered local average temperature, DO, and log biomass density by their overall means, but kept temperature and DO trend variables uncentered to maintain interpretability. We tested additional covariates, including local changes in fishing intensity, but we have not included them in the final models because they did not change our conclusions (see Supplementary Methods).

Simulation study

We conducted a simulation study to assess: (1) the ability of the geostatistical models to cope with the high levels of spatial covariance inherent in spatial grid-based climate and biomass estimates, and (2) to what extent similarities in climate and biotic spatial gradients were responsible for the observed patterns in the velocity-based models. We simulated biomass trends for each species as random fields using the true variance and spatial correlation parameters estimated for each species. Next, we assessed how well our trend-based model accounted for spatial autocorrelation among grid-based estimates by re-fitting the trend-based model using four unique iterations of the simulated data and contrasting the effect sizes and number of species that showed a significant relationship with climate trends in the observed vs. simulated models. If the spatial random effects were effective in preventing type I errors, the trend-based models using simulated data should not show a significant effect of climate more than expected by chance. In the case of velocities, we used the ratio of the simulated biomass trends to the observed spatial gradients in biomass to simulate biotic velocities (henceforth, 'time-null' velocities). This approach maintains the relationships between spatial gradients in biomass and climate that are likely to occur because both species abundances and climate on the seafloor are correlated with depth. Rather than being a test of spatial autocorrelation, these time-null velocities were used to test how important the gradient component was to the results of the fitted velocity model.

Null models based on simulated biotic trends and observed climate trends showed fewer significant relationships at the species level than would be expected by chance (Figures S1, S2, and S3), confirming that the spatial random effects in our models (e.g., Figure S4) successfully controlled for the spatial autocorrelation. In contrast, models predicting time-null biotic velocities did produce more significant effects then would be expected by chance (Figures S5, S6, and S7 vs. S8). These associations were likely due to the simulated velocities being based on the observed spatial gradients (Figure S9); however, comparisons between the velocity model and time-null models suggest that some patterns cannot be accounted for by similarities in the spatial gradients and can be reliably attributed to variation in temporal trends (differences between areas encompassed in black vs. grey violins for interaction terms in Figure 2b). This is in contrast to the complete overlap in black and grey violins for DO velocity in Figure 2b, which indicates that any set of species with identical overall distributions and population variability, but completely random biomass trends, would be likely to show just as many significant species-specific effects. Taken together, these simulations suggest that the velocity model effectively combines both the temporal and spatial dimensions of biotic and climate change, which provides support for our choice to focus on this approach.

Life-history and ecological correlates of climate sensitivity

To assess potential ecological mechanisms and the extent to which the temporal and spatial scales considered were appropriate for the different species, we used mixed-effect models to assess concordance between species' life-history traits and ecology and the estimated effect of climate velocity. We first assessed the independent effects of mean population age (among immature pop-

ulations only) and occupied depth (mean and range). We then tested for independent relationships between climate sensitivity and ecological groupings (including range limits, foraging zones, trophic level, and sociality), while controlling for the depth total ranges occupied (see Supplementary Methods).

Results

Climate trends and velocities

We estimated bottom temperature and DO values biennially between late May and early August during 2008–2018 or 2007–2019, depending on the surveyed area. Seafloor temperature varied from 4.6 °C to 10.2 °C (95% quantile range) across 4×4 km grid cells that had a mean depth within the 99th quantile range of sampled depths (23 to 1112 m). For the same range of survey depths, DO ranged between 0.7 ml/L and 5.7 ml/L (95% quantiles). For both temperature and DO, the highest values were associated with the shallowest depths, while the lowest values were associated with the deepest locations (Figure 1b, c).

Over this period, summer seafloor temperature increased by an average of 0.6 °C per decade across the entire region (95% quantile range of -0.2 to 1.8 °C per decade; Figure 1d). In contrast, the direction of change in seafloor DO was more variable (95% quantiles: -2.8 to 0.6 ml/L per decade; Figure 1e). Warming tended to be most pronounced in the already warmer locations—mean of 1.3 °C/decade in cells shallower than 50 m (Figure S10b). Likewise, the greatest decreases in DO occurred in the shallowest locations (mean: -2 ml/L per decade); however, the highest variability in DO trend (95% quantiles: -1.7 to 0.6 ml/L per decade) occurred between 50 and 200 m depths (Figure S10e). There was a tendency for the shallowest depths to be occupied by groundfish species that have narrower depth ranges (e.g., Southern Rock Sole, *Lepidopsetta billineta*, vs. Dover Sole, *Microstomus pacificus*; Figure S10g, Table S1).

When these local climate trends were placed in their geographic context by converting to gradient-based velocity estimates (Eq. 12), they implied that an organism would have to move an average of 10.5 km/decade (mean of absolute values) to maintain its starting thermal environment and an average of 11 km/decade to maintain initial DO levels. Temperature velocities averaged positive, representing warming conditions (mean: 10.1; 95% interquantile range of -12 to 87; Figure 1f), while DO velocities averaged negative, representing declining DO levels (-6.26; -91 to 24; Figure 1g). Most locations of high climate velocity occurred in patches throughout Queen Charlotte Sound and Hecate Strait (dark red patches in Figure 1f). The most negative DO velocities occurred in shallower portions of Hecate Strait (largest green patch in Figure 1g). The largest velocities tended to be found across a broader range of depths than the largest climate trends (Figure S10).

Linking biotic changes with climate

Geostatistical models linking climatic (Figure 1d–g) and biotic trends (Figures S12 and S13) or velocities (Figures S14 and S15) resolved different aspects of biotic change (Figures S4 and S8). The effect of temperature velocity on biotic velocity was weakly positive across species (β: 0.28 km/decade

with 95% CI -0.04 to 0.60; point range for "T change" shown in Figure 2b), despite a significant overall 0.55% decline in biomass (-0.87 to -0.22) per 1 SD increase in warming (0.8 °C per decade) based on local temperature trend only (point range for "T change" shown in Figures 2a). However, mean local temperature influenced the effect of temperature velocity on biotic velocity (β: -1.09, -1.48 to -0.70; "T interaction" in Figure 2b), such that when temperature velocity was high in the warmest parts of a species' range, local biomass was more likely to decline and exhibit larger negative or smaller positive biotic velocities. When temperature velocity was high in the coolest parts of a species range, local biomass was more likely to increase, and to result in smaller negative or larger positive biotic velocities.

Interactions between mean climate and climate velocity for each maturity class of each species can be illustrated as the predicted relationships between climate and biotic velocities at different mean local conditions (e.g., in Figures 3c and S11a, the blue and red lines are the predicted relationships for locations at the 0.025 and 97.5 quantile of mean local temperatures, respectively). For Redbanded Rockfish (*Sebastes babcocki*) the horizontal blue line indicates stable biomass (small absolute biotic velocities), while the red line with a negative slope means that biomass was more likely to be declining across a local area where conditions were warmest on average and getting warmer across more of the surrounding area (Figure 3b). The slopes of all predicted relationships (e.g., as illustrated in Figure 3c and Figure S11a) are plotted for all species-maturity combinations in Figure 4. Consistent with the overall interaction, the majority of species-maturity combinations with significant interactions between local mean temperature and temperature velocity had negative interactions (31 of 33 coloured dots and lines with red coefficients to the left of blue coefficients in Figure 4a). Over a third of these cases predicted a positive effect of increased temperature velocities for both the warmest and coolest locations, but that the relationship was more strongly positive in the cooler locations (13 of 31 species-maturity combinations with negative interactions).

To assess whether these relationships predicted that specific species' biotic velocities were increasing or decreasing under different climate velocities, the lines displayed in Figures 3c and S11a can be "sliced" at either the minimum temperature velocity experienced by each species (left end of lines) or at the maximum (right end of lines). The expected biotic velocity was near zero for most species-maturity combinations in locations experiencing minimum climate velocity (Figure 5a) regardless of mean temperature. However, the expected biotic velocity was strongly negative for a number of species-maturity combinations (19 of 69) in the warmest locations when experiencing maximum climate velocity and tended to be positive in cooler locations experiencing the same high climate velocity (e.g., Pacific Halibut, *Hippoglossus stenolepis*; Figure 5b).

After controlling for temperature, the average effect of DO velocity on biotic velocity was negative across species (β: -0.48 km/decade, -0.82 to -0.15; point and range for "DO change" in Figure 2b) despite there being a positive effect of DO trend on biomass trend (β: 0.34 % increase in biomass, 0.16 to 0.52; point and range for "DO change" in Figure 2a). Thus, while increasing DO was associated with increases in biomass at a local scale, DO velocity was not on average correlated with biotic velocities. However, unlike for temperature, DO velocity did not interact with mean DO availability consistently across species (β: 0.25, -0.05 to 0.55). Only two species (those with green point ranges on the positive side of the x-axis in Figure 4b) showed the expected interaction

where locations with lower mean DO levels experiencing positive DO velocities were associated with increases in biotic velocity and/or negative DO velocities were associated with decreases in biotic velocity (e.g., immature Lingcod, *Ophiodon elongatus*; Figure 3). In contrast, several species experienced declines in biotic velocity when DO velocity increased across the range of mean DO levels (black point ranges on negative side of x-axis in Figure 4b).

Life-history and ecological correlates of climate sensitivity

We examined possible relationships between responses to climate velocities and each species' taxonomy, traits, and depth distributions. Relationships with biotic velocities that were negative at high temperatures or positive at low temperatures occurred in members of both the largest families represented in our analysis, Sebastidae (rockfish) and Pleuronectidae (righteye flounders) suggesting no strong patterns of similarity among species belonging to the same genus or family (Figures 4a and S8; see also non-significant family-level effects from hierarchical model, Figure S16). However, the effects of temperature velocities at high temperatures were most negative for Chondrichthyan biotic velocities (-1.8 km/decade per SD in temperature velocity, same units apply elsewhere) and rockfish species occupying shelf habitats (-1.3), neutral for continental slope rockfish (0.1) and flatfish (-0.1), and most positive for sablefish (1.0; mean across red values in Figure 4a).

Life-history failed to explain substantial variation in climate sensitivity in the warmest locations, although more negative effects tended to be clustered in shallow depths and among younger immature populations (Figure S17). However, the positive effects of temperature velocities on biotic velocities in the coolest locations were strongest in species occupying a larger range of depths (β: 0.57, 0.21 to 0.92) and for immature populations with younger mean age (β: -1.0, -2.0 to 0). Ecological factors were somewhat better at accounting for negative effects in the warmest locations. The effects of temperature velocity at high mean temperatures differed significantly between species depending on diet (lower biotic velocities in zooplantivores than species at higher trophic levels; β: -0.96, -1.44 to -0.48), and use of foraging zones (higher biotic velocities in demersal species relative to benthopelagic; β: 0.98, 0.47 to 1.49) after accounting for mean depth occupied (Figure S18 top row). The strongest negative effects of warming temperature velocities (estimated for the warmest parts of a species distribution) were for species occurring at intermediate depths, whereas most species with mean encounter depths deeper than 290 m appeared to increase in biotic velocity with more positive temperature velocities (Figure S19c).

In contrast, DO velocities at low mean DO locations only showed a strong positive effect on Lingcod biotic velocities (0.7) and negative effects were strongest for both continental slope rockfish (-1.1) and flatfish (-1.4; mean across green values in Figure 4b). These negative relationships represent declining biotic velocity with increasing DO, or visa versa, and tended to be stronger both for species occupying deeper locations on average (β: -0.43, -0.73 to -0.13; Figure S19d) and a larger range of depths (β: -0.30, -0.6 to 0). It is notable, however, that the effect of trends in DO on percent change in biomass were also negative at these depths despite being mostly positive at intermediate depths (Figure S19b). At these intermediate depths (the mean occupied depth for

species in this analysis of about 175 m), the effects of DO velocity at low DO was also most negative for species foraging at higher trophic levels (β: -0.33, -0.81 to 0.16), in the demersal zone (β: -0.79, -1.32 to -0.26), and with more solitary habits (β: -0.63, -1.21 to -0.06; Figure S18 bottom row).

Discussion

Using novel geostatistical models fit to bottom temperature, DO, and demersal fish biomass from scientific trawl surveys, we related trends and velocities between climatic and biotic variables across 38 species. Local declines in demersal fish biomass were, on average, associated with warming trends and decreases in DO. However, after converting trends to velocities, a clear interaction between temperature velocity and mean bottom temperature emerged. On average, and for roughly half the species-maturity combinations, temperature velocity had a more negative effect on biotic velocity in already warm locations than in relatively cool locations. Converting these interaction effects into expected values, approximately one quarter of species-maturity combinations experienced declines (negative biotic velocities) in the warmest locations when experiencing maximum warming. In contrast, locations experiencing minimal warming or cool locations experiencing maximum warming experienced stable or increasing biotic velocities. Characteristics such as trophic level, foraging zone, and sociality—as well as potentially confounding variables such as commercial fishing effort or catch—explained little of the observed effects. Although DO velocity results were more equivocal, planktivores responded more positively to DO velocity under low DO conditions (Figure S18f) than species with more diverse or higher trophic-level diets. This suggests that the prevalence of strong negative relationships between DO and biotic velocities (Figure 2b) might be explained by increases in primary production in benthic environments, causing decreases in DO due to increased rates of decomposition (Keister *et al.* 2020).

Our analysis is the first, to our knowledge, to explore how the interaction between climate velocities and local mean climate conditions affect fine-scale biotic velocities, and the first to contrast patterns between trend and velocity indices. Globally, the impact of temperature change in marine environments appears to be highly dependent on local mean temperatures, whether measured in range shifts relative to temperature velocity (e.g., Lenoir *et al.* 2020) or species richness and abundance in response to temperature trends (e.g., Antão *et al.* 2020). Specifically, this latter meta-analysis of patterns in marine taxa found that abundance was positively correlated with warming, except in the warmest of locations (Antão *et al.* 2020). While our trend model indicated an overall negative effect of rising temperatures on local fish density, the velocity model was consistent with the global pattern in showing that most negative relationships occurred only in already warm locations (Figure 2). Large climate velocities reflect more spatially uniform environments—where an organism would need to move greater distances to maintain constant climate—and likewise, small velocities reflect more spatially heterogeneous environments (Loarie *et al.* 2009). As a result, more spatially uniform regions have greater weight in the velocity model than in the trend model, and this stretching and compressing of trend values based on spatial heterogeneity likely explains why the negative interactive effect of mean temperature was only detected for velocities. Overall, we focused primarily on the velocity results since they represent a more ecologically

meaningful measure than trends alone, given that they account for the local reality species face if tracking a constant environment (Brito-Morales *et al.* 2018) or prey that themselves track the environment.

For many species, we do not know how far individuals travel on a daily or seasonal basis, so uncertainty remains as to the extent to which the modelled spatial resolution is appropriate for each of the species in this analysis. While the trend- and velocity-based models capture slightly different spatial scales (4 × 4 km focal cell vs. 12 × 12 km encompassed when considering patterns among neighbouring cells as well), both resolutions are smaller than what is often used for analyses of climate change in the marine environment (Oestreich *et al.* 2020, Pinsky *et al.* 2020), substantial environmental changes can occur at even smaller scales, and these local-scale effects may be especially important for species with high site fidelity (e.g., Yelloweye Rockfish *Sebastes ruberrimus*, Hannah and Rankin 2011). However, in order to detect the impact of climate change on rockfish (many of which have generation times > 20 yrs), one would require either data in excess of 20 years, or to contrast patterns of change between age classes. Indeed, responses to environmental change can be expected to differ between species, depending on the life history of species including physiological tolerances, lifespan, and dispersal patterns (Massiot-Granier *et al.* 2018). Furthermore, reaching reproductive maturity frequently results in shifts in dispersal patterns, habitat selectivity, physiological tolerances (Laurel *et al.* 2007), and therefore represents a potentially important break point for understanding the impacts of climate change. Given the relatively short timescale encompassed in our analysis (one decade), we expected to find stronger patterns in shorter-lived/immature portions of populations and more pelagic species. Within immature populations, those with a younger mean age were found to exhibit the most extreme responses to temperature velocity (positive in coolest locations and negative in warmest locations; Figure S17c); however, immature populations did not have overall stronger responses than mature populations (Figure S22b). Ecological responses were somewhat complicated by interactions with depths occupied; but, contrary to expectation, more extreme responses tended to belong to demersal foraging and solitary species, rather than those with more pelagic or schooling behaviours (Figure S18c, g, h).

Aggregate metrics such as the centre of gravity have also demonstrated that demersal fishes use both shifts in latitude and depth to track changes in ocean temperatures (e.g., Perry *et al.* 2005, Dulvy *et al.* 2008, Li *et al.* 2019), but evidence that range edges on the North American continental shelf have shifted further north than expected or even contracted southward, suggest roles for competition, climate-independent mortality and/or density-dependent habitat selection (Li *et al.* 2019, Fredston *et al.* 2020). Indeed, fishing pressure on the Atlantic shelf was found to be more important than average bottom temperature for predicting centre of gravity for five groundfish species, despite temperature being more correlated with variance in biomass (Adams *et al.* 2018). This latter result suggests that there was spatial variability in temperature, or responses to temperature, which were not fully captured by the centre of gravity (VanDerWal *et al.* 2013). Fine-scale local effects may contribute to the relatively greater influence of temperature relative to fishing pressure in our analysis. Groundfish species in the eastern Bering Sea also do not show a strong correlation even for local climate and biotic velocities, but no interaction with mean conditions

was reported (Alabia *et al.* 2018). Another potential explanation for stronger negative effects on Canadian Pacific groundfish is that species here are closer to the southern ends of their distributions and may therefore be closer to the warm end of their temperature tolerances, especially in the warmest locations. However, although we found the strongest negative biotic velocities in these warmer locations, species nearer to their northern range limit were not more likely to show a positive response to temperature.

There are a number of limitations to our analysis. First, our analysis cannot separate fish movement in response to climate from a host of other possible explanations. For example, local changes in biomass density can be a result of movement, local population growth, age cohorts beyond our two maturity categories, changes in average body size (Shackell *et al.* 2010, Laurel *et al.* 2007), or effects of fishing not captured by the metrics of total catch or hours fished. Indeed, some of the hypothesized effects of warming climate and lower DO on fishes include higher metabolism and ability to store fat, reduced productivity, and slower growth resulting in generally smaller fish (Klein *et al.* 2017, Madeira *et al.* 2017). Furthermore, changes in local density may be correlated with climate, not because of groundfish thermal preference, but because groundfish seek prey or avoid predators that have themselves shifted their distribution in response to climate. Second, there are limitations to our data. The CTD climate data from Canadian Pacific trawl surveys are only available from 2008 onward, the surveys occur in one seasonal period (May to August) and cover a given region only once every two years. Also, some of the species (e.g., shallower rockfish species) may be better sampled by longline gear than trawl gear. This spatial and temporal scope will miss overlap in major life-history events for some species (e.g., Sablefish; Beamish 2008), or seasonal movements (e.g., Pacific Halibut; Loher 2011). Importantly, the input data for our meta-analytic model are predictions from our first-stage geostatistical models. Third, it is possible that climate conditions may themselves affect survey catchability. For example, groundfish may flee gear more slowly or aggregate to avoid low DO conditions (Craig 2012), thereby making fish more catchable and biasing observations.

Our work suggests multiple future research directions. First, future efforts may aim to identify common spatial patterns across species using spatial dimension reduction tools such as spatial factor analysis (Thorson *et al.* 2015a). Areas where species overlap in their response would represent important areas for conservation (Brito-Morales *et al.* 2018), but also areas where competition may be expected to increase or new fisheries interactions may occur. Second, some rockfish are better sampled by longline survey gear and future analyses could use such survey data, or combine survey data from multiple gear types (Webster *et al.* 2020), to develop a composite density estimate. Third, our analysis used CTD data, which was only available for spring or summer from 2008 onwards and required a statistical model to extrapolate to the full region. An alternative would be a ROMS (Regional Ocean Modeling System) model (Peña *et al.* 2019), which could extend the temporal scope, allow for accounting of climate at other times of the year (e.g., temperature during spawning; Laurel and Rogers 2020), allow for inclusion of variables not typically measured with survey data (e.g., primary production), and allow for forward projections. Preliminary investigations indicated a strong correlation between our CTD projections and recently updated ROMS bottom temperatures. With the greater spatial and temporal extent that ROMS data will provide,

calculation of more geographically precise analog-based climate velocities could be used to further refine the identification of areas important for conservation (Brito-Morales *et al.* 2018).

Climate change is expected to have large impacts on fish stocks and their management, particularly with respect to changes in species distribution (e.g., Tommasi *et al.* 2017, Karp *et al.* 2019, Free *et al.* 2019). Legislation and policy in jurisdictions around the world (e.g., the US *Magnuson-Stevens Act*, Canada's *Fisheries Act*, the European Marine Strategy Framework Directive) require that environmental conditions affecting fish stocks be accounted for in management decisions such as setting sustainable catch limits and developing rebuilding plans. However, there is often a mismatch between scale of climate predictions, the scale at which species respond, and the scale of management decisions (Stock *et al.* 2011, Maureaud *et al.* 2021). For example, the populations analyzed in this study are managed at the mesoscale, with catch limits often determined for individual substocks (DFO 2019). The metrics presented in our paper represent fine-scale indicators of response to a changing environment, which are useful for assessing risk and conservation planning (Brito-Morales *et al.* 2018). Shifts in distribution, such as those reported here, can have implications for calculation of indices of abundance, and estimates of stock size and stock status, which in turn may impact harvest recommendations (Szuwalski and Hollowed 2016, Karp *et al.* 2019). Analyses such as ours can be incorporated into frameworks for improving advice for the management of fisheries under climate change (e.g. Plagányi *et al.* 2011, Punt *et al.* 2014, Karp *et al.* 2019).

Acknowledgements

We thank Fisheries and Oceans Canada's Aquatic Climate Change Adaptation Services Program (ACCASP) for funding that supported this work. We thank E.A. Keppel, G.D. Workman, and M.R. Wyeth for helpful discussions and assistance with data extraction. We thank P.L. Thompson for comments that substantially improved this manuscript. We thank the many individuals who have contributed to collecting the synoptic survey data on which this manuscript is based (available at https://open.canada.ca/).

Data Availability Statement

The biological data that support the findings of this study are openly available through open.canada.ca at https://open.canada.ca/data/en/dataset/a278d1af-d567-4964-a109-ae1e84cbd24a and the associated environmental measurements are available on request.

References

Adams, C.F., Alade, L.A., Legault, C.M., O'Brien, L., Palmer, M.C., Sosebee, K.A. and Traver, M.L. (2018) Relative importance of population size, fishing pressure and temperature on the spatial distribution of nine Northwest Atlantic groundfish stocks. *PLOS ONE* **13**, e0196583.

Alabia, I.D., Molinos, J.G., Saitoh, S.I., Hirawake, T., Hirata, T. and Mueter, F.J. (2018) Distribution shifts of marine taxa in the Pacific Arctic under contemporary climate changes. *Diversity and Distributions* **24**, 1583–1597.

Anderson, S.C., Keppel, E.A. and Edwards, A.M. (2019) A reproducible data synopsis for over 100 species of British Columbia groundfish. *DFO Can. Sci. Advis. Sec. Res. Doc.* **2019/041**. URL http://www.dfo-mpo.gc.ca/csas-sccs/Publications/ResDocs-DocRech/2019/2019_041-eng.html.

Anderson, S.C., Ward, E.J., English, P.A. and Barnett, L.A.K. (2020) *sdmTMB: Spatiotemporal Species Distribution GLMMs with 'TMB'*. URL https://github.com/pbs-assess/sdmTMB. R package version 0.0.11.9000.

Antão, L.H., Bates, A.E., Blowes, S.A., Waldock, C. *et al.* (2020) Temperature-related biodiversity change across temperate marine and terrestrial systems. *Nature Ecology and Evolution* **4**, 927–933.

Barbeaux, S.J. and Hollowed, A.B. (2018) Ontogeny matters: Climate variability and effects on fish distribution in the eastern Bering Sea. *Fisheries Oceanography* **27**, 1–15.

Beamish, R.J. (2008) Impacts of climate and climate change on the key species in the fisheries in the North Pacific. *North Pacific Marine Science Organization* .

Bell, R.J., Odell, J., Kirchner, G. and Lomonico, S. (2020) Actions to promote and achieve climate-ready fisheries: summary of current practice. *Marine and Coastal Fisheries* **12**, 166–190.

Bizzarro, J., Yoklavich, M. and Wakefield, W. (2017) Diet composition and foraging ecology of U.S. Pacific Coast groundfishes with applications for fisheries management. *Environmental Biology of Fishes* **100**.

Brito-Morales, I., García Molinos, J., Schoeman, D.S., Burrows, M.T. *et al.* (2018) Climate Velocity Can Inform Conservation in a Warming World. *Trends in Ecology & Evolution* **33**, 441–457.

Brown, C. and Schoeman, D. (2020) *vocc: Functions for Calculating the Velocity of Climate Change*. URL https://github.com/cbrown5/vocc. R package version 0.1.1.

Burrows, M.T., Schoeman, D.S., Buckley, L.B., Moore, P. *et al.* (2011) The pace of shifting climate in marine and terrestrial ecosystems. *Science* **334**, 652–655.

Carroll, C., Lawler, J.J., Roberts, D.R. and Hamann, A. (2015) Biotic and Climatic Velocity Identify Contrasting Areas of Vulnerability to Climate Change. *PLOS ONE* **10**, e0140486.

Comte, L. and Grenouillet, G. (2015) Distribution shifts of freshwater fish under a variable climate: Comparing climatic, bioclimatic and biotic velocities. *Diversity and Distributions* **21**, 1014–1026.

Craig, J.K. (2012) Aggregation on the edge: effects of hypoxia avoidance on the spatial distribution of brown shrimp and demersal fishes in the Northern Gulf of Mexico. *Marine Ecology Progress Series* **445**, 75–95.

Cressie, N.A.C. and Wikle, C.K. (2011) *Statistics for Spatio-Temporal Data*. Wiley Series in Probability and Statistics. Wiley, Hoboken, N.J.

DFO (2019) Pacific region integrated fisheries management plan, groundfish, effective february 21, 2019, version 1.1. .

Doney, S.C., Ruckelshaus, M., Emmett Duffy, J., Barry, J.P. *et al.* (2012) Climate change impacts on marine ecosystems. *Annual Review of Marine Science* **4**, 11–37.

Dulvy, N.K., Rogers, S.I., Jennings, S., Stelzenmüller, V., Dye, S.R. and Skjoldal, H.R. (2008) Climate change and deepening of the North Sea fish assemblage: A biotic indicator of warming seas. *Journal of Applied Ecology* **45**, 1029–1039.

Dunn, P.K. and Smyth, G.K. (2005) Series evaluation of Tweedie exponential dispersion model densities. *Statistics and Computing* **15**, 267–280.

Fredston, A., Pinsky, M., Selden, R., Szuwalski, C., Thorson, J., Halpern, B. and Gaines, S. (2020) Range edges of North American marine species are tracking temperature over decades. Preprint: https://doi.org/10.22541/au.160331933.33155622/v1.

Fredston-Hermann, A., Selden, R., Pinsky, M., Gaines, S.D. and Halpern, B.S. (2020) Cold range edges of marine fishes track climate change better than warm edges. *Global Change Biology* **26**, 2908–2922.

Free, C.M., Thorson, J.T., Pinsky, M.L., Oken, K.L., Wiedenmann, J. and Jensen, O.P. (2019) Impacts of historical warming on marine fisheries production. *Science* **363**, 979–983.

Frölicher, T.L., Fischer, E.M. and Gruber, N. (2018) Marine heatwaves under global warming. *Nature* **560**, 360.

Frölicher, T.L. and Laufkötter, C. (2018) Emerging risks from marine heat waves. *Nature Communications* **9**, 650.

García Molinos, J., Halpern, B., Schoeman, D., Brown, C. *et al.* (2016) Climate velocity and the future global redistribution of marine biodiversity. *Nature Climate Change* **6**, 83–88.

Godefroid, M., Boldt, J.L., Thorson, J.T., Forrest, R. *et al.* (2019) Spatio-temporal models provide new insights on the biotic and abiotic drivers shaping Pacific Herring (*Clupea pallasi*) distribution. *Progress in Oceanography* **178**, 102198.

Hamann, A., Roberts, D.R., Barber, Q.E., Carroll, C. and Nielsen, S.E. (2015) Velocity of climate change algorithms for guiding conservation and management. *Global Change Biology* **21**, 997–1004.

Hannah, R.W. and Rankin, P.S. (2011) Site fidelity and movement of eight species of Pacific rockfish at a high-relief rocky reef on the Oregon coast. *North American Journal of Fisheries Management* **31**, 483–494.

Hare, J.A., Alexander, M.A., Fogarty, M.J., Williams, E.H. and Scott, J.D. (2010) Forecasting the dynamics of a coastal fishery species using a coupled climate–population model. *Ecological Applications* **20**, 452–464.

Karp, M.A., Peterson, J.O., Lynch, P.D., Griffis, R.B. *et al.* (2019) Accounting for shifting distributions and changing productivity in the development of scientific advice for fishery management. *ICES Journal of Marine Science* **76**, 1305–1315.

Keister, J.E., Winans, A.K. and Herrmann, B. (2020) Zooplankton Community Response to Seasonal Hypoxia: A Test of Three Hypotheses. *Diversity* **12**, 21.

Klein, E.S., Smith, S.L. and Kritzer, J.P. (2017) Effects of climate change on four New England groundfish species. *Reviews in Fish Biology and Fisheries* **27**, 317–338.

Kristensen, K., Nielsen, A., Berg, C.W., Skaug, H. and Bell, B.M. (2016) TMB: Automatic Differentiation and Laplace Approximation. *J. Stat. Softw.* **70**, 1–21.

Latimer, A.M., Banerjee, S., Sang Jr, H., Mosher, E.S. and Silander Jr, J.A. (2009) Hierarchical models facilitate spatial analysis of large data sets: a case study on invasive plant species in the northeastern United States. *Ecology Letters* **12**, 144–154.

Laurel, B.J. and Rogers, L.A. (2020) Loss of spawning habitat and prerecruits of Pacific cod during a Gulf of Alaska heatwave. *Canadian Journal of Fisheries and Aquatic Sciences* **77**, 644–650.

Laurel, B.J., Stoner, A.W. and Hurst, T.P. (2007) Density-dependent habitat selection in marine flatfish: the dynamic role of ontogeny and temperature. *Marine Ecology Progress Series* **338**, 183–192.

Lenoir, J., Bertrand, R., Comte, L., Bourgeaud, L., Hattab, T., Murienne, J. and Grenouillet, G. (2020) Species better track climate warming in the oceans than on land. *Nature Ecology and Evolution* **4**, 1044–1059.

Li, L., Hollowed, A.B., Cokelet, E.D., Barbeaux, S.J. *et al.* (2019) Subregional differences in groundfish distributional responses to anomalous ocean bottom temperatures in the northeast Pacific. *Global Change Biology* **25**, 2560–2575.

Lindgren, F., Rue, H. and Lindström, J. (2011) An explicit link between Gaussian fields and Gaussian Markov random fields: The stochastic partial differential equation approach. *J. R. Stat. Soc. Ser. B Stat. Methodol.* **73**, 423–498.

Loarie, S.R., Duffy, P.B., Hamilton, H., Asner, G.P., Field, C.B. and Ackerly, D.D. (2009) The velocity of climate change. *Nature* **462**, 1052–1055.

Loher, T. (2011) Analysis of match-mismatch between commercial fishing periods and spawning ecology of Pacific halibut (*Hippoglossus Stenolepis*), based on winter surveys and behavioural data from electronic archival tags. *ICES Journal of Marine Science* **68**, 2240–2251.

Love, M.S. (2011) *Certainly more than you want to know about the fishes of the Pacific Coast: a postmodern experience.* Really Big Press.

Love, M., Yoklavich, M. and Thorsteinson, L. (2002) *The Rockfishes of the Northeast Pacific.* University of California Press.

MacCall, A.D. (1990) *Dynamic geography of marine fish populations.* Washington Sea Grant Program Seattle, WA.

Madeira, C., Mendonça, V., Leal, M.C., Flores, A.A., Cabral, H.N., Diniz, M.S. and Vinagre, C. (2017) Thermal stress, thermal safety margins and acclimation capacity in tropical shallow waters—An experimental approach testing multiple end-points in two common fish. *Ecological Indicators* **81**, 146 – 158.

Massiot-Granier, F., Lassalle, G., Almeida, P.R., Aprahamian, M. *et al.* (2018) A generic method to assess species exploratory potential under climate change. *Ecological Indicators* **90**, 615–623.

Masson, D. and Fine, I. (2012) Modeling seasonal to interannual ocean variability of coastal British Columbia. *Journal of Geophysical Research: Oceans* **117**.

Maureaud, A.A., Frelat, R., Pécuchet, L., Shackell, N. *et al.* (2021) Are we ready to track climate-driven shifts in marine species across international boundaries? A global survey of scientific bottom trawl data. *Global Change Biology* **27**, 220–236.

Mindel, B.L., Webb, T.J., Neat, F.C. and Blanchard, J.L. (2016) A trait-based metric sheds new light on the nature of the body size–depth relationship in the deep sea. *Journal of Animal Ecology* **85**, 427–436.

Molinos, J.G., Schoeman, D.S., Brown, C.J. and Burrows, M.T. (2019) VoCC: An R package for calculating the velocity of climate change and related climatic metrics. *Methods in Ecology and Evolution* **10**, 2195–2202.

Morley, J.W., Selden, R.L., Latour, R.J., Frölicher, T.L., Seagraves, R.J. and Pinsky, M.L. (2018) Projecting shifts in thermal habitat for 686 species on the North American continental shelf. *PLOS ONE* **13**, e0196127.

Nye, J.A., Link, J.S., Hare, J.A. and Overholtz, W.J. (2009) Changing spatial distribution of fish stocks in relation to climate and population size on the Northeast United States continental shelf. *Marine Ecology Progress Series* **393**, 111–129.

Oestreich, W.K., Chapman, M.S. and Crowder, L.B. (2020) A comparative analysis of dynamic management in marine and terrestrial systems. *Frontiers in Ecology and the Environment* **18**, 496–504.

Okey, T.A., Alidina, H.M., Lo, V. and Jessen, S. (2014) Effects of climate change on Canada's Pacific marine ecosystems: a summary of scientific knowledge. *Reviews in Fish Biology and Fisheries* **24**, 519–559.

Oldfather, M.F., Kling, M.M., Sheth, S.N., Emery, N.C. and Ackerly, D.D. (2020) Range edges in heterogeneous landscapes: Integrating geographic scale and climate complexity into range dynamics. *Global Change Biology* **26**, 1055–1067.

Ordonez, A. and Williams, J.W. (2013) Projected climate reshuffling based on multivariate climate-availability, climate-analog, and climate-velocity analyses: Implications for community disaggregation. *Climatic Change* **119**, 659–675.

Parmesan, C. and Yohe, G. (2003) A globally coherent fingerprint of climate change impacts across natural systems. *Nature* **421**, 37–42.

Perry, A.L., Low, P.J., Ellis, J.R. and Reynolds, J.D. (2005) Climate change and distribution shifts in marine fishes. *Science* **308**, 1912–1915.

Peterson, W., Robert, M. and Bond, N. (2015) The warm blob-conditions in the northeastern Pacific Ocean. *PICES Press* **23**, 36.

Peña, M.A., Fine, I. and Callendar, W. (2019) Interannual variability in primary production and shelf-offshore transport of nutrients along the northeast Pacific Ocean margin. *Deep Sea Research Part II: Topical Studies in Oceanography* **169-170**, 104637.

Pinsky, M.L., Rogers, L.A., Morley, J.W. and Frölicher, T.L. (2020) Ocean planning for species on the move provides substantial benefits and requires few trade-offs. *Science Advances* **6**, eabb8428.

Pinsky, M.L. and Fogarty, M. (2012) Lagged social-ecological responses to climate and range shifts in fisheries. *Climatic Change* **115**, 883–891.

Pinsky, M.L., Worm, B., Fogarty, M.J., Sarmiento, J.L. and Levin, S.A. (2013) Marine taxa track local climate velocities. *Science* **341**, 1239–1242.

Plagányi, É.E., Weeks, S.J., Skewes, T.D., Gibbs, M.T. *et al.* (2011) Assessing the adequacy of current fisheries management under changing climate: A southern synopsis. *ICES Journal of Marine Science* **68**, 1305–1317.

Pörtner, H.O., Roberts, D.C., Masson-Delmotte, V., Zhai, P. *et al.* (2019) *IPCC special report on the ocean and cryosphere in a changing climate.* Cambridge University Press.

Punt, A.E., A'mar, T., Bond, N.A., Butterworth, D.S. *et al.* (2014) Fisheries management under climate and environmental uncertainty: Control rules and performance simulation. *ICES Journal of Marine Science* **71**, 2208–2220.

Pörtner, H., Bock, C., Knust, R., Lannig, G., Lucassen, M., Mark, F. and Sartoris, F. (2008) Cod and climate in a latitudinal cline: physiological analyses of climate effects in marine fishes. *Clim. Res.* **37**, 253–270.

R Core Team (2019) *R: A Language and Environment for Statistical Computing*. R Foundation for Statistical Computing, Vienna, Austria.

Rindorf, A. and Lewy, P. (2006) Warm, windy winters drive cod north and homing of spawners keeps them there. *Journal of Applied Ecology* **43**, 445–453.

Rooper, C.N., Ortiz, I., Hermann, A.J., Laman, N., Cheng, W., Kearney, K. and Aydin, K. (2020) Predicted shifts of groundfish distribution in the Eastern Bering Sea under climate change, with implications for fish populations and fisheries management. *ICES Journal of Marine Science* .

Royer, T.C. (1998) Coastal processes in the northern North Pacific. *The Global Coastal Ocean : Regional Studies and Synthesis* Publisher: John Wiley.

Rue, H., Martino, S. and Chopin, N. (2009) Approximate Bayesian inference for latent Gaussian models by using integrated nested Laplace approximations. *Journal of the Royal Statistical Society: Series B (Statistical Methodology)* **71**, 319–392.

Serra-Diaz, J.M., Franklin, J., Ninyerola, M., Davis, F.W., Syphard, A.D., Regan, H.M. and Ikegami, M. (2014) Bioclimatic velocity: The pace of species exposure to climate change. *Diversity and Distributions* **20**, 169–180.

Shackell, N.L., Frank, K.T., Fisher, J.A.D., Petrie, B. and Leggett, W.C. (2010) Decline in top predator body size and changing climate alter trophic structure in an oceanic ecosystem. *Proceedings of the Royal Society B: Biological Sciences* **277**, 1353–1360.

Shelton, A.O., Thorson, J.T., Ward, E.J. and Feist, B.E. (2014) Spatial semiparametric models improve estimates of species abundance and distribution. *Canadian Journal of Fisheries and Aquatic Sciences* **71**, 1655–1666.

Sinclair, A., Schnute, J., Haigh, R., Starr, P., Rick Stanley, Jeff Fargo and Workman, G. (2003) Feasibility of multispecies groundfish bottom trawl surveys on the BC coast. DFO Canadian Science Advisory Secretariat (CSAS) Research Document 2003/049.

Stock, C.A., Alexander, M.A., Bond, N.A., Brander, K.M. *et al.* (2011) On the use of IPCC-class models to assess the impact of climate on Living Marine Resources. *Progress in Oceanography* **88**, 1–27.

Sunday, J.M., Pecl, G.T., Frusher, S., Hobday, A.J. *et al.* (2015) Species traits and climate velocity explain geographic range shifts in an ocean-warming hotspot. *Ecology Letters* **18**, 944–9530.

Szuwalski, C.S. and Hollowed, A.B. (2016) Climate change and non-stationary population processes in fisheries management. *ICES Journal of Marine Science* **73**, 1297–1305.

Thorson, J.T. and Barnett, L.A.K. (2017) Comparing estimates of abundance trends and distribution shifts using single- and multispecies models of fishes and biogenic habitat. *ICES Journal of Marine Science* .

Thorson, J.T., Fonner, R., Haltuch, M.A., Ono, K. and Winker, H. (2017) Accounting for spatiotemporal variation and fisher targeting when estimating abundance from multispecies fishery data. *Canadian Journal of Fisheries and Aquatic Sciences* **74**, 1794–1807.

Thorson, J.T., Pinsky, M.L. and Ward, E.J. (2016a) Model-based inference for estimating shifts in species distribution, area occupied and centre of gravity. *Methods in Ecology and Evolution* , 990–1002.

Thorson, J.T., Rindorf, A., Gao, J., Hanselman, D.H. and Winker, H. (2016b) Density-dependent changes in effective area occupied for sea-bottom-associated marine fishes. *Proceedings of the Royal Society B: Biological Sciences* **283**, 20161853.

Thorson, J.T., Scheuerell, M.D., Shelton, A.O., See, K.E., Skaug, H.J. and Kristensen, K. (2015a) Spatial factor analysis: a new tool for estimating joint species distributions and correlations in species range. *Methods in Ecology and Evolution* **6**, 627–637.

Thorson, J.T., Shelton, A.O., Ward, E.J. and Skaug, H.J. (2015b) Geostatistical delta-generalized linear mixed models improve precision for estimated abundance indices for West Coast groundfishes. *ICES Journal of Marine Science* **72**, 1297–1310.

Tommasi, D., Stock, C.A., Hobday, A.J., Methot, R. *et al.* (2017) Managing living marine resources in a dynamic environment: The role of seasonal to decadal climate forecasts. *Progress in Oceanography* **152**, 15–49.

Turris, B.R. (2000) A comparison of British Columbia's ITQ fisheries for groundfish trawl and sablefish: Similar results from programmes with differing objectives, designs and processes. *FAO Fisheries Technical Paper* , 254–261.

Tweedie, M.C.K. (1984) An index which distinguishes between some important exponential families. In: *Statistics: Applications and New Directions. Proceedings of the Indian Statistical Institute Golden Jubilee International Conference* (eds. J.K. Gosh and J. Roy). Indian Statistical Institute, Calcutta, pp. 579–604.

VanDerWal, J., Murphy, H.T., Kutt, A.S., Perkins, G.C., Bateman, B.L., Perry, J.J. and Reside, A.E. (2013) Focus on poleward shifts in species' distribution underestimates the fingerprint of climate change. *Nature Climate Change* **3**, 239–243.

Wallace, S., Turris, B., Driscoll, J., Bodtker, K., Mose, B. and Munro, G. (2015) Canada's Pacific groundfish trawl habitat agreement: A global first in an ecosystem approach to bottom trawl impacts. *Marine Policy* **60**, 240–248.

Ward, E.J., Jannot, J.E., Lee, Y.W., Ono, K., Shelton, A.O. and Thorson, J.T. (2015) Using spatiotemporal species distribution models to identify temporally evolving hotspots of species co-occurrence. *Ecological Applications* **25**, 2198–2209.

Webster, R.A., Soderlund, E., Dykstra, C.L. and Stewart, I.J. (2020) Monitoring change in a dynamic environment: spatiotemporal modelling of calibrated data from different types of fisheries surveys of pacific halibut. *Canadian Journal of Fisheries and Aquatic Sciences* 77, 1421–1432.

Williams, D.C., Nottingham, M.K., Olsen, N. and Wyeth, M.R. (2018) Summary of the Queen Charlotte Sound synoptic bottom trawl survey, July 6 – August 8, 2015. *DFO Can. Manuscr. Rep. Fish. Aquat. Sci.* **3136**, viii + 64 p.

Yang, M.S., Dodd, K., Hibpshman, R. and Whitehouse, A. (2006) Food habits of groundfishes in the Gulf of Alaska in 1999 and 2001. *NOAA Technical Memorandum* , 13.

Tables

Table 1: Gradient-based velocity metrics and their definitions. Climatic variables are temperature and dissolved oxygen (DO); biotic variables are biomass density for the mature and immature components of a species. Climatic and biotic variables are represented generically by A. Our analysis treated gradient-based velocity as a scalar, using only the magnitude component of the velocity vector.

Term	Notation	Definition	Magnitude	Sign
Local trend	$m_s^A = \frac{\Delta A_s}{\Delta t}$	Change in local biotic or climatic scalar A per decade	Temporal rate of change in A	Increasing (+) or decreasing (−) local trend in A
Spatial gradient	$\vec{g}_s^A$	Vector sum (magnitude, angle) of mean north or south and east or west gradients of A in a 3×3 cell spatial neighbourhood	Spatial rate of change in A	Vector magnitude and angle always positive (+)
Gradient-based velocity	$\vec{V}_s^A = \frac{m_s^A}{\vec{g}_s^A}$	Vector velocity (magnitude, angle) from local trend of A divided by vector local spatial gradient of A	Speed of travel predicted to maintain initial A	Increasing (+) or decreasing (−) based on the local trend in A

Figures

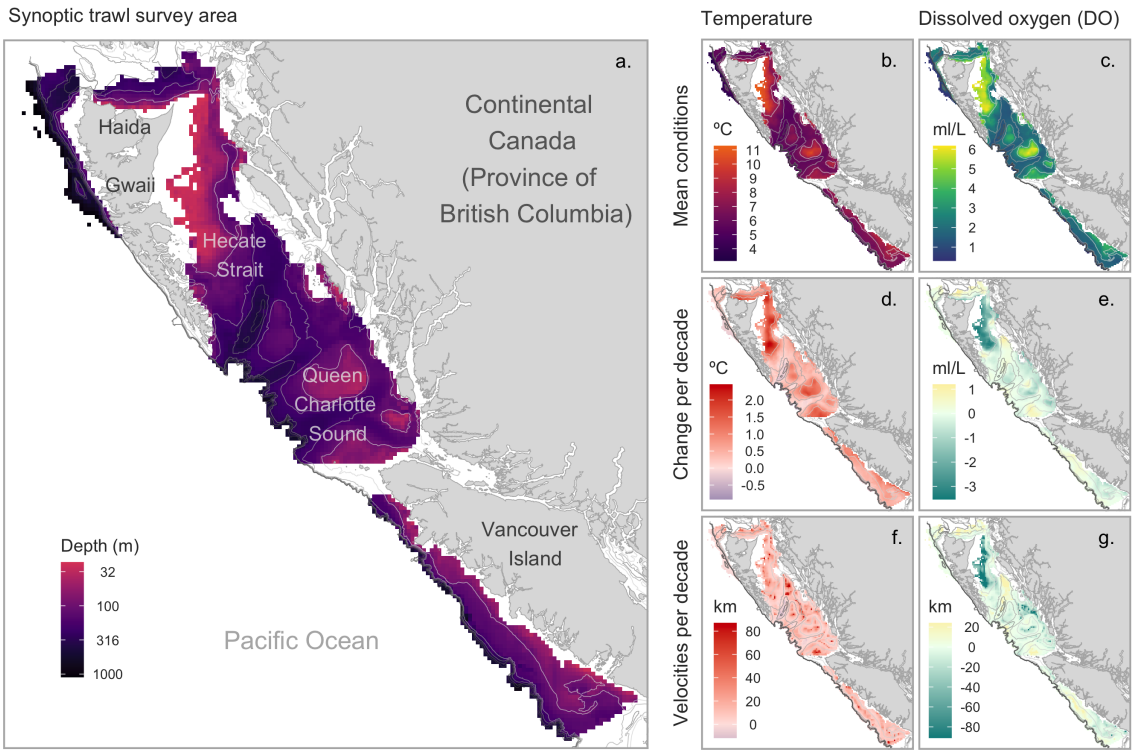

Figure 1: Maps of study area (a), predicted mean conditions (b, c), decadal trends (d, e), and decadal velocities (f, g) of bottom temperature and dissolved oxygen (DO) for 2008–2018 off the coast of British Columbia, Canada. Values are estimated using geostatistical spatiotemporal models of CTD sensor data collected during late-spring/early-summer groundfish trawl surveys. Bathymetry lines at every 100 m are overlaid in shades of grey that increase with depth.

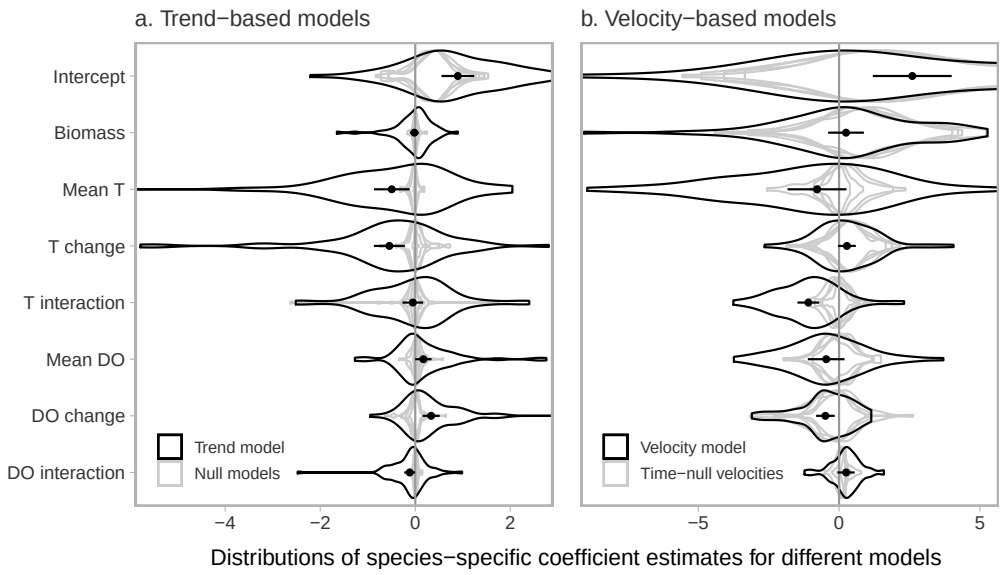

Figure 2: Distribution of species-specific (random effect) coefficients from the model fitted to observed data (black violins) compared with coefficients from four simulated null models (gray violins). Each "violin" is based on a single model including all species (a: trend-based models where climate and biotic change variables are all local trends; b: velocity models where climate and biotic change variables are all velocities). Black points with ranges represent the observed-data global (fixed effect) coefficient estimates with 95% CIs. Null models used fitted covariate values, but simulated response data. Simulated time-null velocities used these same simulated trends divided by the real spatial gradients. The x-axes have been truncated slightly for interpretability.

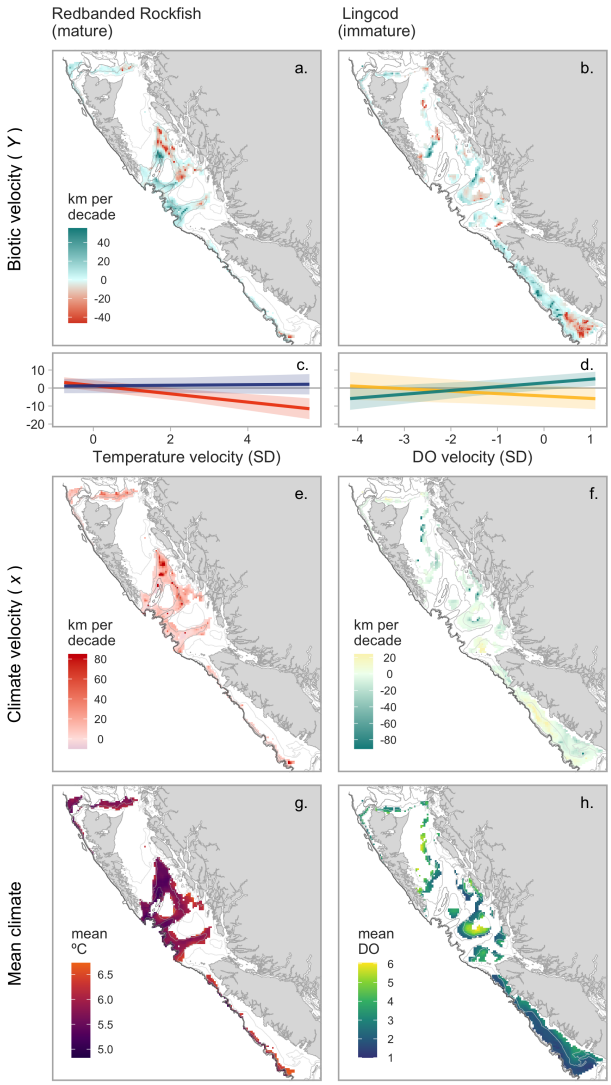

Figure 3: Maps and interaction plots for two illustrative species representing the most frequent relationship with temperature (left column) and the expected response with DO (right column). Mature *Sebastes babcocki* had stable, near-zero, biotic velocities regardless of amount of warming in the coolest regions it occupied, and decreases in biomass when temperatures increased in warmer regions (a,c,e,g). Immature *Ophiodon elongatus* biotic velocities increased with positive DO velocities in low mean DO locations only (b,d,f,h). In panel c, a blue line represents predicted biotic velocity (Y, y-axis) for different temperature velocities (x, x-axis) in the coolest locations (0.025 quantile of those occupied by 95% of the estimated biomass of each species) and a red line represents the same for the warmest locations (0.975 quantile). Likewise, for predictions at different DO velocities, green represents the lower quantile of mean DO and yellow the higher (d). Both the colours and slopes illustrated correspond with those in Figure 4. The maps include biotic velocity estimates for all locations that cumulatively account for 95% of the estimated biomass of each species (a, b), and the same climate estimates as in Figure 1, but trimmed to include only the values for the same locations as the biotic velocities for each species predicted relationships.

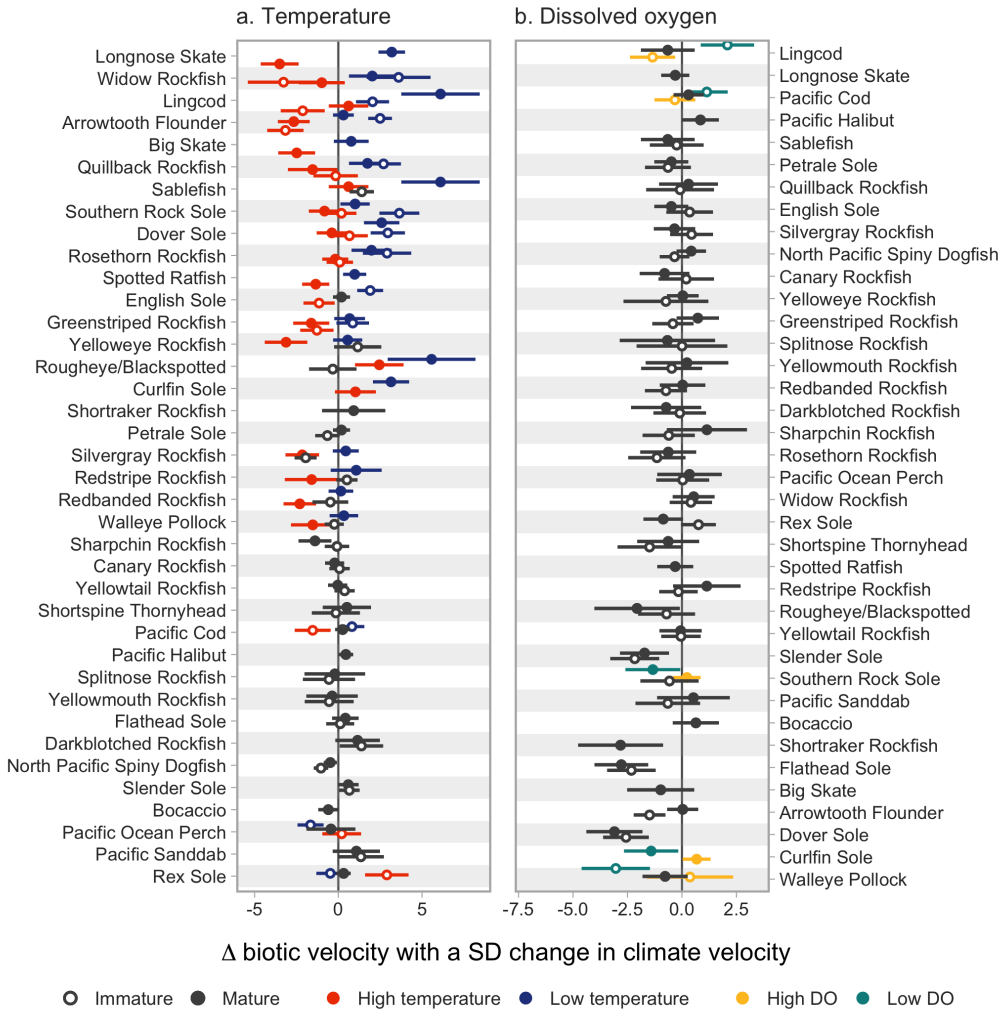

Figure 4: Mean climate and climate change interact in predicting biotic velocities (km/decade) for 38 groundfish species. Coloured dot-whiskers indicate slopes and 95% CIs of the predicted biotic velocities with 1 SD of change in climate velocity for the low and high 95% quantiles of mean local climate (i.e., the slopes of lines in interaction plots like those in Figure 3c, d). Species are ordered by the difference between the slopes at the highest and lowest quantiles of mean climate such that the more intuitive results are at the top: increases in climate velocity have a more positive impact on biotic velocity when starting at a low mean temperature (a) or DO level (b). Open circles indicate patterns for immature fish and closed circles represent individuals large enough to have a 50% chance of having reached reproductive maturity, or belonging to species for which maturity data was not available. Black dot-whiskers represent the slopes for each maturity class when the interaction is not significant.

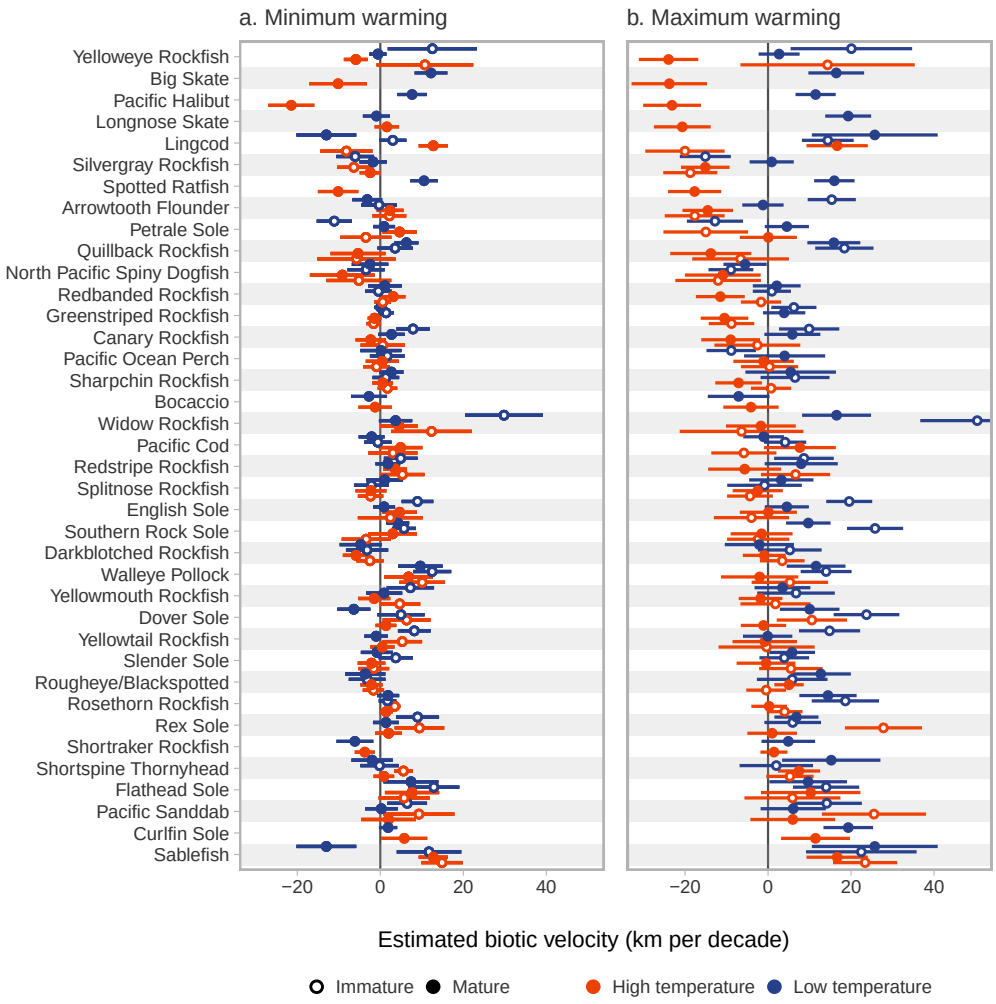

Figure 5: Estimates of biotic velocities (km/decade with 95% CI) for 38 groundfish species under different mean temperatures (blue and red represent low and high 95% quantiles) occupied and at (a) the minimum and (b) maximum temperature velocities experienced for each species. Open circles indicate patterns for immature fish and closed circles represent individuals large enough to have a 50% chance of being reproductively mature, or belonging to species for which maturity data were not available. Species are ordered by the minimum estimates at the maximum climate velocity experienced for each species. Therefore, species most likely to experience population declines with increasing temperatures are at the top.

Supporting Methods, Tables, and Figures

Maturity and length-weight models

When maturity data were collected for a species in all years for all surveys (> 250 samples across all years and > 40 each year), we included a random intercept for year to allow for temporal change in size at maturity:

$$M_i \sim \text{Bernoulli}\left(p_i\right), \tag{17}$$

$$p_i = \text{logit}^{-1}\left(\alpha + \alpha_t + \beta L_i\right), \tag{18}$$

$$\alpha_t \sim \text{Normal}\left(0, \sigma_\alpha^2\right), \tag{19}$$

where M_i represents the mature (1) or immature (0) status of fish i, p_i represents the probability of maturity of fish i, α represents a global intercept, α_t represents a year-specific deviation for year t that is allowed to vary with a variance of σ_α^2, β represents a coefficient, and L_i represents the length of fish i. We used year-specific 50% maturity probability thresholds to split observed catches into maturity classes. For species not meeting the above thresholds, we used a random effect of tow instead of year, and split catches based on the global estimate.

For all catches exceeding the species-specific threshold count of individual fish on a survey, either a random subset of roughly 50 fish or all individuals were measured for both length and weight. We therefore filled in occasional missing weights as

$$\log(W_i) \sim \text{Student-t}\left(3, \log(a) + b\log(L_i), \sigma\right), \tag{20}$$

with W_i and L_i representing the weight and length for fish i, a and b being the species-specific parameter estimates of the length-weight relationship $W_i = aL_i^b$, σ representing the observation error scale, and 3 representing a degrees of freedom parameter fixed to allow for outlying residuals.

Alternative spatiotemporal models of fish biomass density

We tried including the proportion of muddy sediment and proportion of sediment with any rocks as covariates in biomass density models, but the values we used were likely not specific enough to the trawl path sampled, and therefore not helpful to our models. Certainly more spatially precise estimates would be possible with refined substrate variables, but likely irrelevant to this analysis given the resolution and uncertainty in our climate variables. Furthermore, the spatial random effects can account for spatial factors that are constant across time, like substrate type, while spatiotemporal random effects account for factors that vary from year to year spatially such as bottom temperature, water circulation patterns, species interactions, and species movement.

Velocity calculation considerations

An alternative to gradient-based velocity calculations is to search for analogous conditions in the second time period and calculate the shortest actual distance to an analogous cell. This method requires a threshold of change below which cells are deemed analogous which is often derived from historical variability in climate. We calculated analog-distance velocities that were qualitatively similar to gradient-based velocities by using twice the minimum standard deviation of each climate variable as our threshold and time periods defined by prior-to and post onset of the same marine

heatwave. However, models including these values tended to have more difficulty converging, so we relied instead on the gradient-based values and the component values for all our analyses (Figs 1 and S9).

Alternative model configurations for linking biotic changes with climate

We tested additional covariates that we chose not to include in the final model. We calculated average hours fished by commercial bottom trawl for each 4×4 km grid cell per year between 2008 and 2018, as well as the percent change in time spent fishing during this time (Figure S20). The log of mean fishing intensity, the trend in fishing intensity, and the interaction between the two were all included as covariates in a climate trend model, but none of these variables showed any more significant negative relationships than might be expect by chance (Figure S21). We tested for an overall effects of maturity (treating mature fish as the intercept) on the main effects of all climate variables (all two-way interactions), and on the interactions (model with 3-way interactions). For each maturity class of each species, the model estimated an independent random spatial field either with or without genus or family as taxonomic grouping factors (Figure S16); however, final models do not include any grouping factors because they did not change any of the model estimates qualitatively. Finally, we attempted to assess the importance of the gradient component in velocity estimates by adding temperature gradient to a model of biomass change in response to temperature trends, and including a three-way interaction between temperature trend, mean, and gradient. None of the important effects we focus on in the results (Figure S22) were changed qualitatively by any of these added variables.

How climate sensitivity varies with life history

We calculated weighted means and interquartile ranges of depths from maturity-specific biomass densities for all survey catches. Because climate conditions experienced vary with depth and a narrower species depth range might increase other ecological effects, we include these variables as covariates. From the individual fish caught in these trawl surveys, we calculated the maximum recorded body mass of each species and average age (estimated from otoliths or fin clips when available) for each maturity class of each species Given that age data were available for only a subset of species , we first assessed the independent effects of mean population ageand occupied depth (mean and range) on species responses to climate (Figure S17). These models also included an interaction with whether the response slope estimated was at the high or low extreme of mean conditions, and a random intercept for species (to capture the non-independence of the estimates for high and low climate extremes). Finally, to reduce leverage of extreme slope estimates, these extreme values were collapsed down to be equal to the 0.005 and 0.995 quantiles of all slope estimates. We then tested for relationships between ecological groupings and slope estimates (at both the high or low extreme of mean conditions) across both maturity classes, while controlling for the mean depth occupied. These models also used collapsed slope estimates (see previous paragraph), included a fixed effect of the mean climate (high or low) that the response slope was estimated for, and a random intercepts for both species and maturity classes nested within species.

How climate sensitivity varies with ecology

The species and life history stages varied with respect to their trophic level, behaviour, and overarching distribution (Table S1). Species were classified into either zooplanktivores or higher trophic level feeders based on the majority of their diet components from available literature (Love *et al.* 2002, Yang *et al.* 2006, Bizzarro *et al.* 2017). Species were classified as solitary and demersal (flatfishes, Lingcod, Sablefish, skates and some rockfishes) or bentho-pelagic and schooling (cods and some rockfishes). Rockfishes were classified based on Love *et al.* (2002). British Columbia occupies a unique oceanographic position at the bifurcation of the North Pacific Current (Royer 1998, Masson and Fine 2012). As such, the distribution of some groundfish species is limited to the north of British Columbia (such as for many of the rockfish species). Although species can occur in Alaska, British Columbia demarcates a northern boundary of relatively high abundance. It was expected that some of the groundfish species in this analysis might be responsive to these larger scale species distribution patterns. Thus, each species was qualitatively categorized based on bottom trawl survey catches in British Columbia, Washington State and Alaska as either occurring in the middle (high catches of the species in all three areas), northern (lowered catches of the species in Southeast Alaska) or southern (lowered catches in Washington State) portions of the species range. There were only three species in the southern portion of their range (Walleye Pollock, Flathead Sole and Arrowtooth Flounder), so in the analysis these were combined with the species in the middle of their distribution.

Table S1: Ecological data for 38 species analyzed, ordered by frequency of occurrence on trawl survey sets between 2008-2018. Classification codes: N = near northern range limit, S = nearer to centre of range or southern limit, L = zooplanktivore, H = all higher trophic diets.

Common name	Scientific name	Sets	Depth occupied (m)				Mean age (years)		Range limit	Trophic level		Foraging zone	Sociality
			Immature		Mature								
			Mean	IQR	Mean	IQR	Imm.	Mat.		Imm.	Mat.		
Arrowtooth Flounder	*Atheresthes stomias*	85%	166	69	168	73	3	10	S	L	H	Demersal	Solitary
Rex Sole	*Glyptocephalus zachirus*	82%	139	55	165	67	-	-	S	H	H	Demersal	Solitary
Spotted Ratfish	*Hydrolagus colliei*	80%	-	-	97	69	-	-	N	-	H	Demersal	Schooling
Dover Sole	*Microstomus pacificus*	74%	167	65	219	145	7	14	S	H	H	Demersal	Solitary
Sablefish	*Anoplopoma fimbria*	55%	232	145	295	220	2	14	S	H	H	Demersal	Solitary
North Pacific Spiny Dogfish	*Squalus suckleyi*	54%	115	61	124	74	-	-	N	L	H	Benthopelagic	Schooling
Pacific Ocean Perch	*Sebastes alutus*	52%	239	56	265	58	6	24	S	L	L	Benthopelagic[+]	Schooling[+]
Pacific Cod	*Gadus macrocephalus*	52%	121	69	125	67	2	4	S	H	H	Benthopelagic	Schooling
Silvergray Rockfish	*Sebastes brevispinis*	46%	181	51	198	60	11	25	N	L	L	Benthopelagic	Solitary
Walleye Pollock	*Gadus chalcogrammus*	46%	133	56	140	73	-	-	S	L	L	Benthopelagic	Schooling
Slender Sole	*Lyopsetta exilis*	44%	156	50	157	52	-	-	N	H	H	Demersal	Solitary
English Sole	*Parophrys vetulus*	44%	72	46	89	43	-	-	N	H	H	Demersal	Solitary
Redbanded Rockfish	*Sebastes babcocki*	41%	257	70	230	62	10	28	S	L	L	Benthopelagic	Solitary
Petrale Sole	*Eopsetta jordani*	41%	117	46	120	48	5	9	N	L	H	Demersal	Solitary
Pacific Halibut*	*Hippoglossus stenolepis*	40%	-	-	110	88	-	-	S	-	H	Demersal	Solitary
Shortspine Thornyhead	*Sebastolobus alascanus*	40%	329	91	352	102	-	-	S	H	H	Demersal	Solitary
Lingcod	*Ophiodon elongatus*	34%	126	51	145	70	3	7	S	H	H	Demersal	Solitary
Longnose Skate*	*Raja rhina*	32%	-	-	222	131	-	-	S	-	H	Demersal	Solitary
Flathead Sole	*Hippoglossoides elassodon*	32%	133	45	131	45	-	-	S	H	H	Demersal	Solitary
Sharpchin Rockfish	*Sebastes zacentrus*	29%	213	50	235	25	7	16	S	L	L	Benthopelagic	Schooling
Greenstriped Rockfish	*Sebastes elongatus*	26%	182	45	173	40	9	26	N	L	L	Demersal	Solitary
Rougheye/Blackspotted Rockfish	*Sebastes aleutianus/melanostictus*	24%	356	50	371	60	16	36	S	H	H	Demersal	Solitary
Redstripe Rockfish	*Sebastes proriger*	23%	134	65	182	50	5	15	S	L	L	Benthopelagic	Schooling
Southern Rock Sole	*Lepidopsetta bilineata*	22%	46	32	50	33	4	8	S	H	H	Demersal	Solitary
Yellowtail Rockfish	*Sebastes flavidus*	22%	116	43	148	36	6	15	N	L	L	Benthopelagic	Schooling
Rosethorn Rockfish	*Sebastes helvomaculatus*	20%	228	65	249	69	-	-	N	H	H	Demersal	Solitary
Canary Rockfish	*Sebastes pinniger*	19%	147	53	164	34	8	18	N	L	L	Benthopelagic	Schooling
Pacific Sanddab	*Citharichthys sordidus*	18%	76	35	83	26	-	-	N	H	H	Demersal	Solitary
Yellowmouth Rockfish	*Sebastes reedi*	15%	217	25	232	46	11	33	N	L	L	Benthopelagic	Schooling
Splitnose Rockfish	*Sebastes diploproa*	14%	250	39	294	33	7	19	N	L	L	Benthopelagic	Schooling
Darkblotched Rockfish	*Sebastes crameri*	11%	256	91	306	48	-	-	N	L	L	Demersal	Solitary
Curlfin Sole**	*Pleuronichthys decurrens*	10%	-	-	58	28	-	-	N	-	H	Demersal	Solitary
Bocaccio**	*Sebastes paucispinis*	10%	-	-	162	38	-	22	N	-	H	Benthopelagic	Solitary
Quillback Rockfish	*Sebastes maliger*	10%	65	21	76	37	6	20	N	L	H	Demersal	Solitary
Yelloweye Rockfish	*Sebastes ruberrimus*	9%	149	39	156	36	-	-	S	L	H	Demersal	Solitary
Big Skate*	*Beringraja binoculata*	9%	-	-	75	58	-	-	S	-	H	Demersal	Solitary
Widow Rockfish	*Sebastes entomelas*	9%	74	82	180	141	2	21	N	L	L	Benthopelagic	Schooling
Shortraker Rockfish**	*Sebastes borealis*	5%	-	-	393	153	-	63	S	-	H	Demersal	Solitary

[+]Immature individuals use the alternate strategy
*Species for which maturity data not collected
**Species not captured frequently enough when immature to fit the spatial model

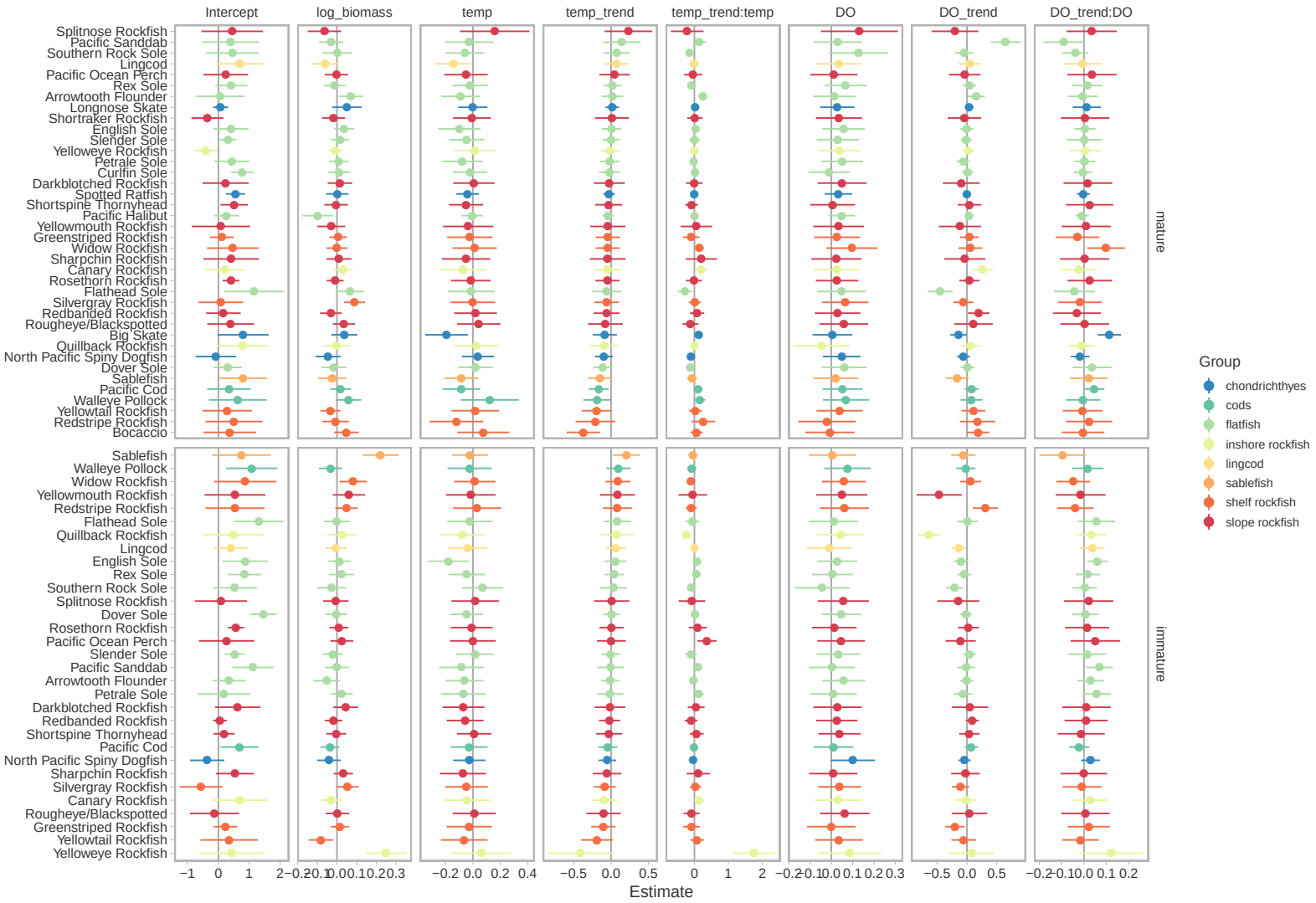

Figure S1: Species-specific coefficient estimates from one example of a simulated trends model (null #1) ordered by the estimated effect of temperature trend.

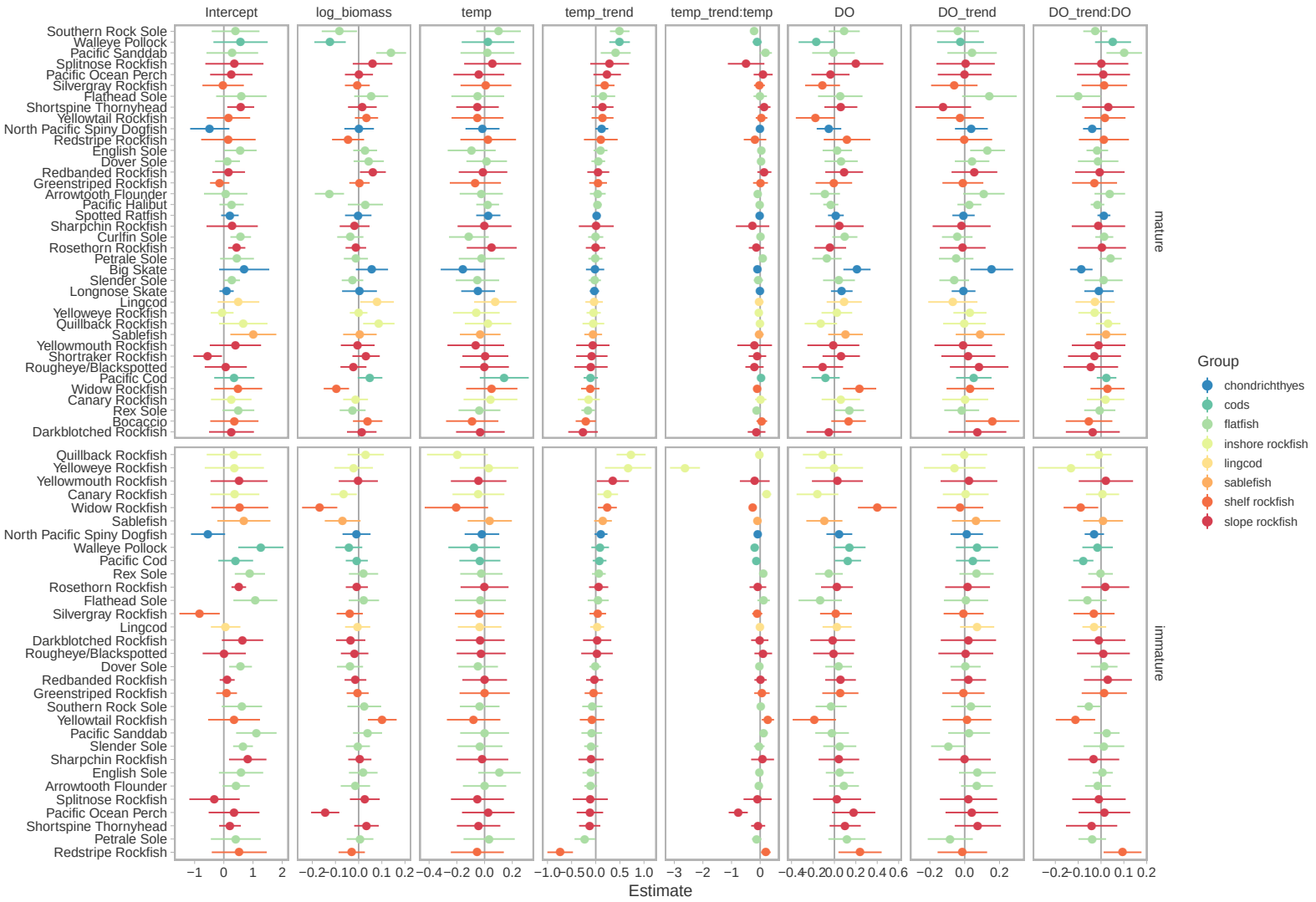

Figure S2: Species-specific coefficient estimates from one example of a simulated trends model (null #2) ordered by the estimated effect of temperature trend.

Figure S3: Species-specific coefficient estimates from one example of a simulated trends model (null #3) ordered by the estimated effect of temperature trend.

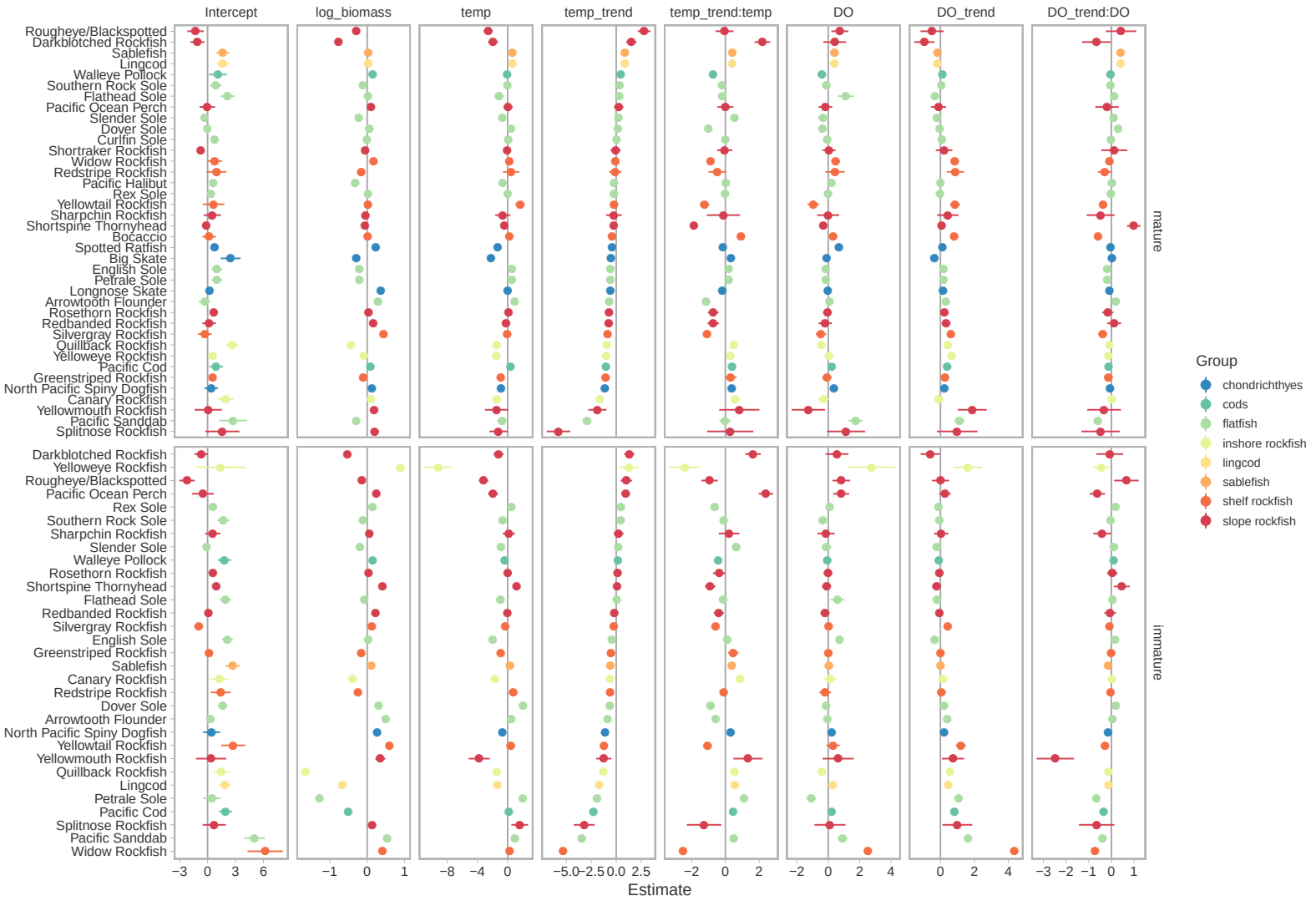

Figure S4: Species-specific coefficient estimates from trend model ordered by the estimated effect of temperature trend for a cell with an average biomass density and climate conditions and with no change in DO.

Figure S5: Species-specific coefficient estimates from one example of a simulated velocity model (null #1) ordered by the estimated effect of temperature velocity. The simulated biotic velocities used for this model were derived from simulated trends and true spatial gradients.

Figure S6: Species-specific coefficient estimates from one example of a simulated velocity model (null #2) ordered by the estimated effect of temperature velocity. The simulated biotic velocities used for this model were derived from simulated trends and true spatial gradients.

Figure S7: Species-specific coefficient estimates from one example of a simulated velocity model (null #3) ordered by the estimated effect of temperature velocity. The simulated biotic velocities used for this model were derived from simulated trends and true spatial gradients.

Figure S8: Species-specific coefficient estimates from velocity model ordered by the estimated effect of temperature velocity, which represents the change in the velocity of biomass change for a cell with an average biomass density and climate conditions and with no change in DO.

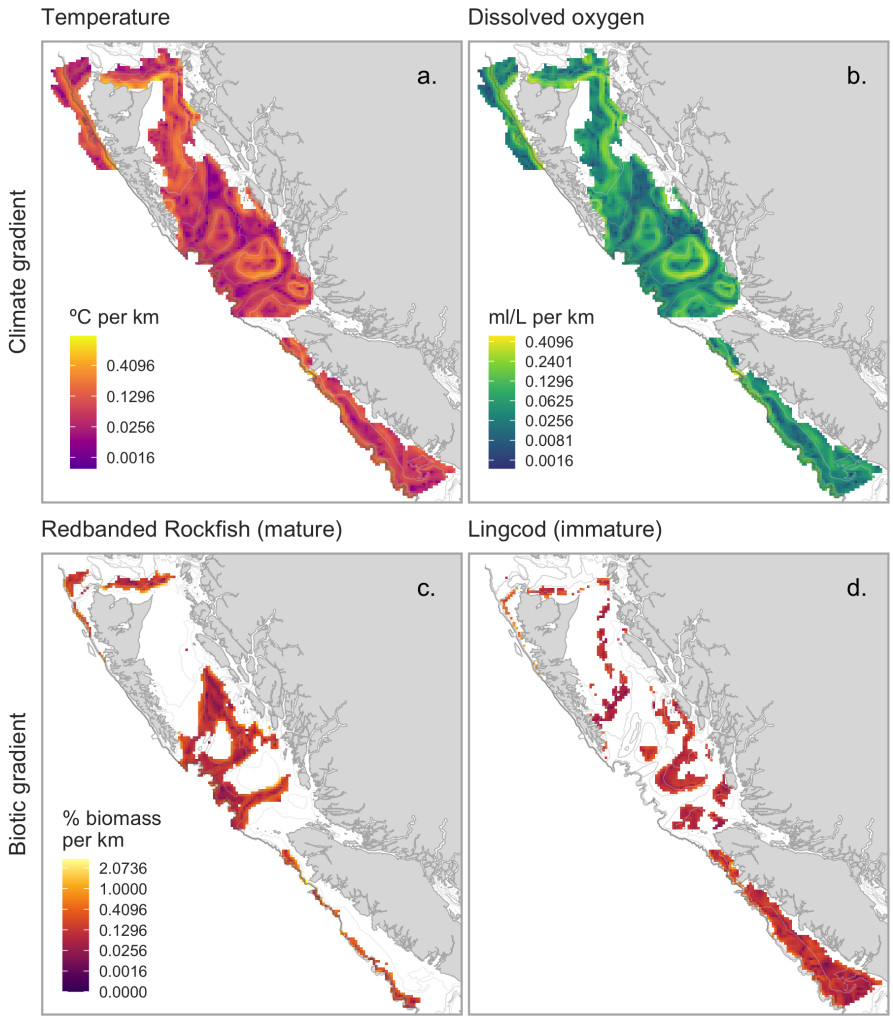

Figure S9: Maps of the gradient component of velocity calculations for both climate and biomass. Biotic gradient panels are for example species.

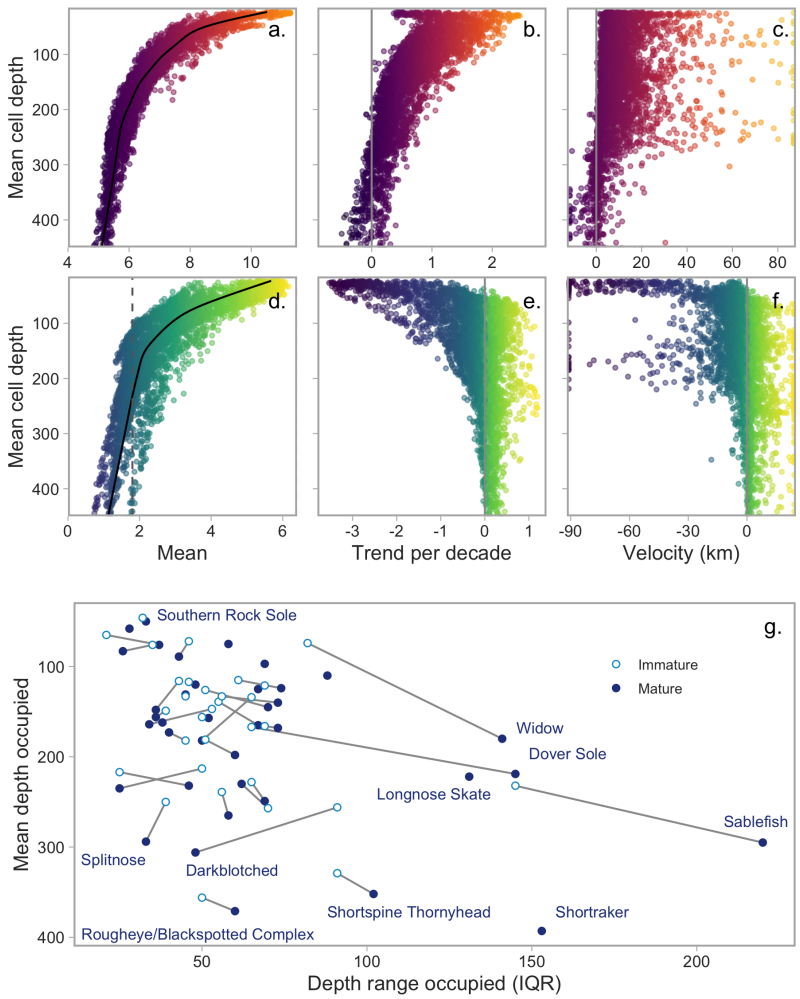

Figure S10: The climate conditions of each cell across depths (y-axes of upper panels) are indicated by both colours and the values on the x-axes of the 6 upper plots. Mean depth occupied by groundfish species co-varies with interquartile depth range occupied (g) and many of these species move deeper (lower on y-axis) with maturity (classes linked by grey lines) often with a corresponding increase in depth range (to right on x-axis).

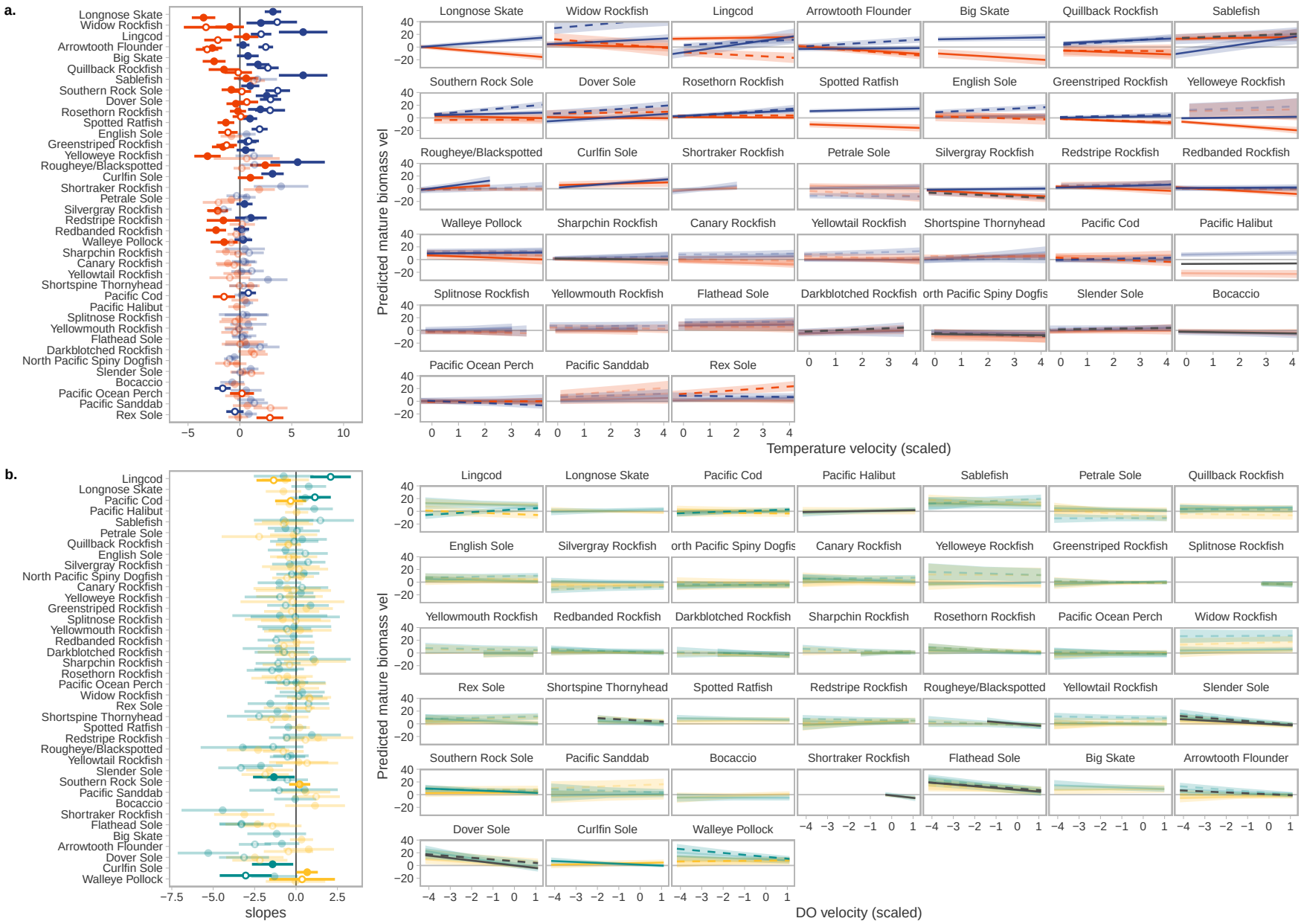

Figure S11: Slopes of predicted biotic **velocity** based on interaction between (a) seafloor temperature **velocity** and the mean temperature, or (b) seafloor DO **velocity** and mean DO levels. Colours, symbols, and order are the same as in Figure **??**.

Figure S12: Biomass trends for mature fish populations (top and bottom 5th quantiles are not included in the colour scale, but are coloured by the nearest scale value).

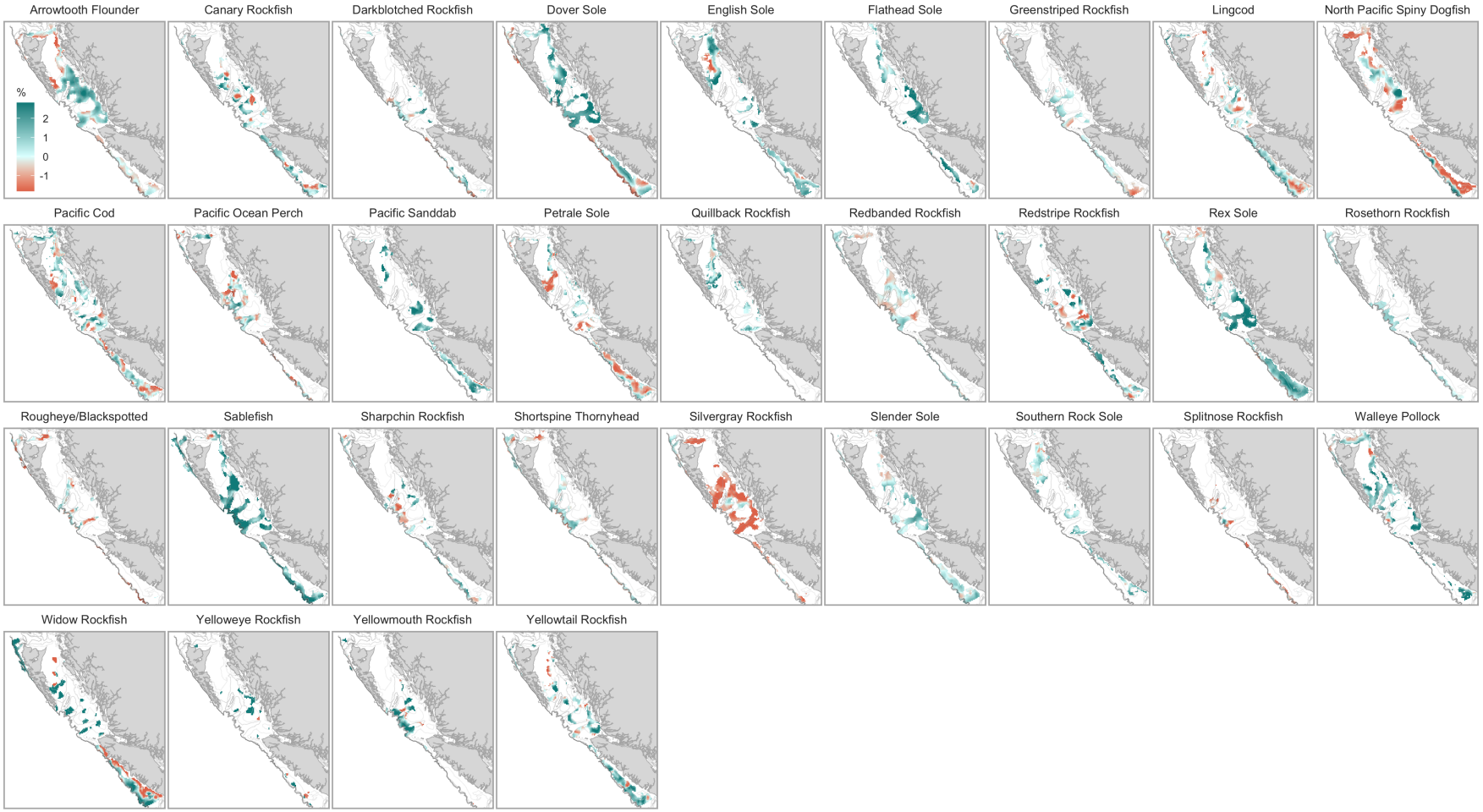

Figure S13: Biomass trends for immature fish populations on same scale as Figure S12.

Figure S14: Biotic velocities for mature fish populations.

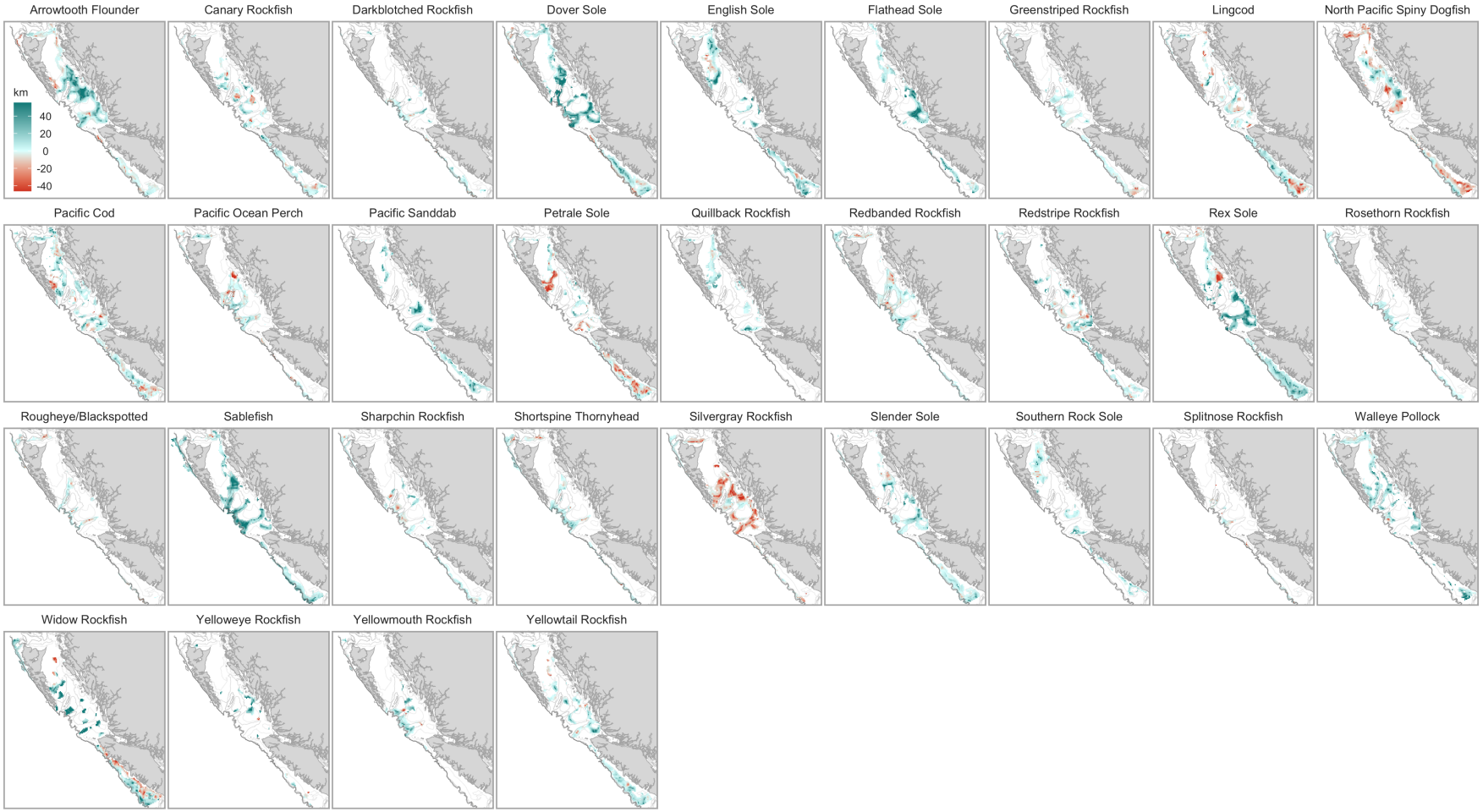

Figure S15: Biotic velocities for immature fish populations.

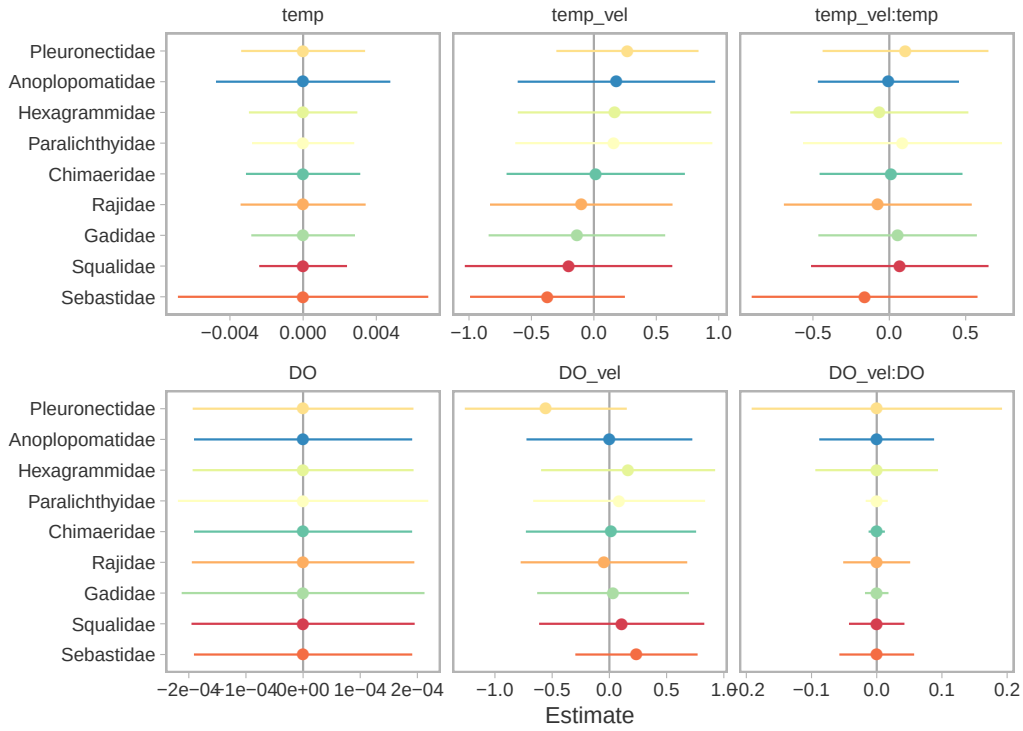

Figure S16: Family-level coefficient estimates for climate variables all have confidence intervals overlapping zero. Families are ordered by decreasing biotic velocity with increasing temperature velocity. This model includes the same climate variables as the "Velocity" models in Figures 2b and S22.

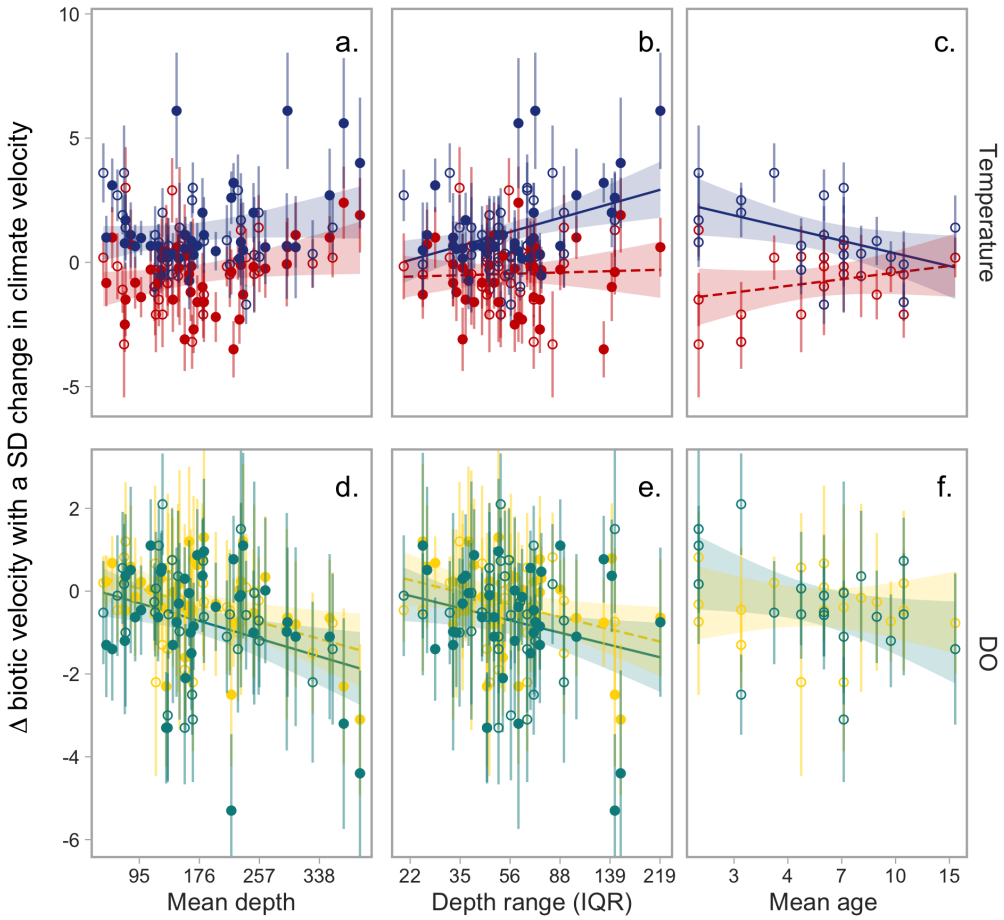

Figure S17: Occupied range of depths and immature population age correlate with the effect of warming temperature velocities on biotic velocities at low temperatures (a-c) and/or DO levels (e). Mean depth occupied only correlated with effects of DO (d). Each panel illustrates a separate model with a random effect of species and a fixed effect of mean local climate as a high or low 95th quantile for temperature or DO levels (colours and shapes match Figure 4). Points with ranges represent each species' raw slope estimates from the spatial models and their CI. Regression lines indicate significant relationships and corresponding uncertainties are based only on fixed-effects, and do not account for uncertainty in the slope estimates.

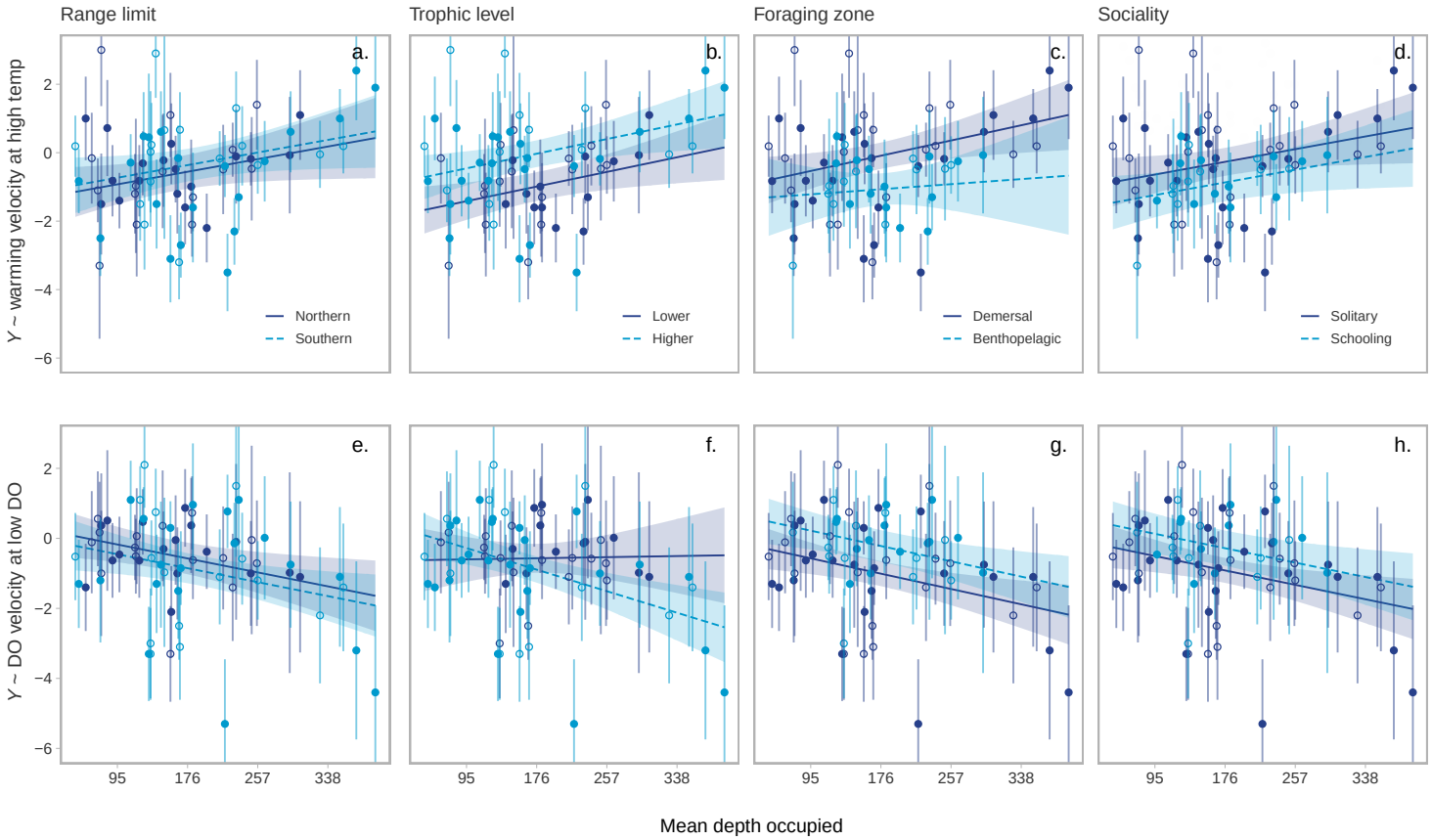

Figure S18: Ecological traits overlaid on responses to climate velocities, while controlling for the mean depth occupied by different maturity classes of each species. Points represent each species' raw slope estimates and their CI from the velocity model each coloured based on species and maturity-class specific ecology, with open circles for immature, and closed circles for mature biomass. Regression lines are derived from mixed-effect models with random intercepts for species and maturity classes nested within species; however, uncertainties are based only on fixed-effects and do not account for uncertainty in the slope estimates. In addition to the variables illustrated, each model contains slopes for both high and low mean conditions, but only the raw data and the estimated relationship for the stronger effect (highest temperatures and lowest DO) are plotted here. An interaction between ecology and mean depth is included only when statistically significant.

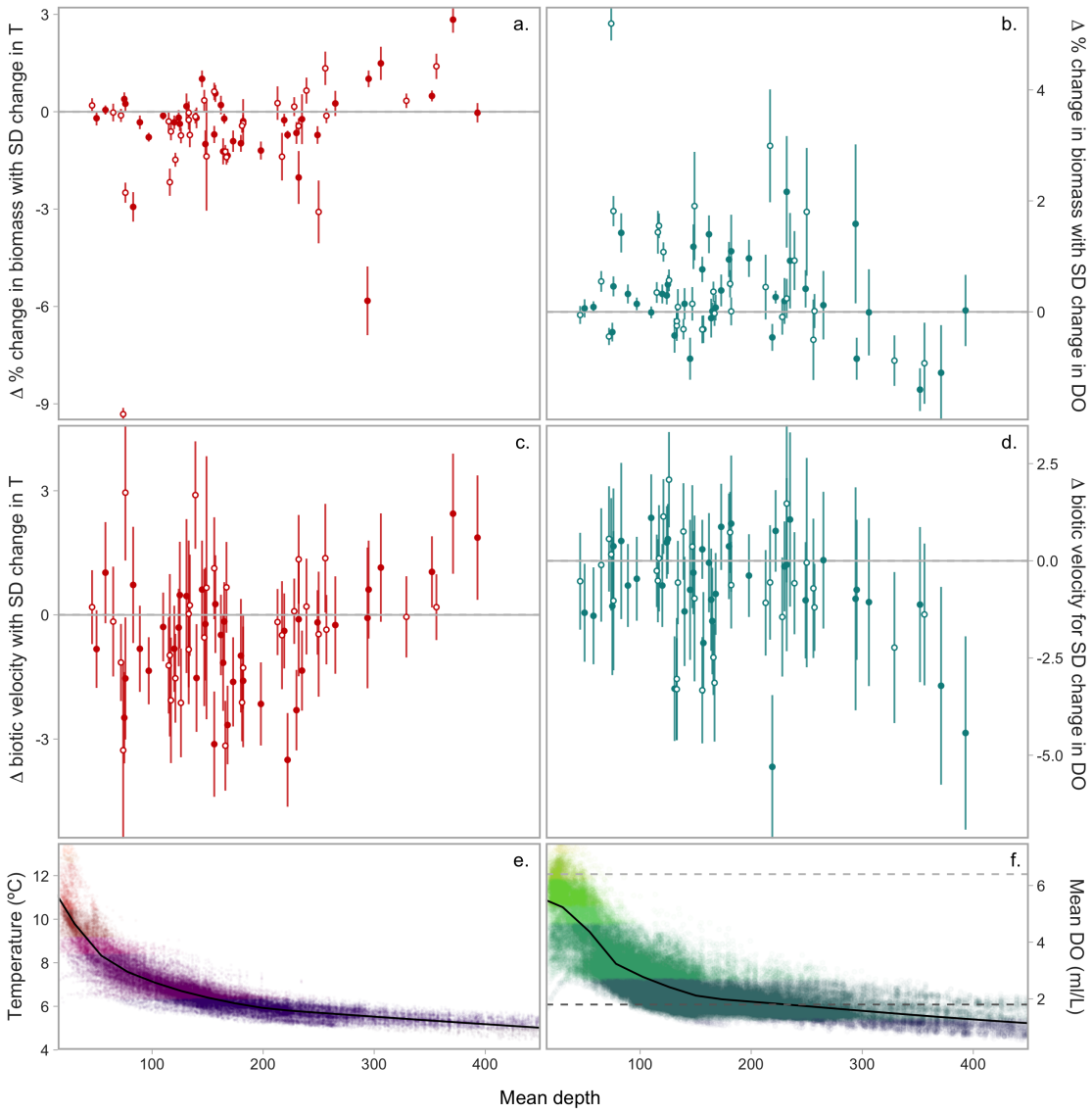

Figure S19: The slopes of the relationship between changes in biomass and climate, when calculated for the environmental extremes expected to have the greatest physiological impact—(b) highest temperature locations and (c) lowest DO locations—do not change predictably with mean occupied depth. Line segments on points represent 95% CIs on slope estimates from spatial models. Bottom panels illustrate relationships (smoothed solid lines are GAMs) between estimated temperature (d) and DO (e) with mean depth in each 4x4 km survey grid cell (dots). Dashed lines (e) represent complete saturation of seawater at 1 bar, 10 degree C, 35 salinity (upper), or threshold for mildly hypoxic conditions (< 1.8 ml/L; lower).

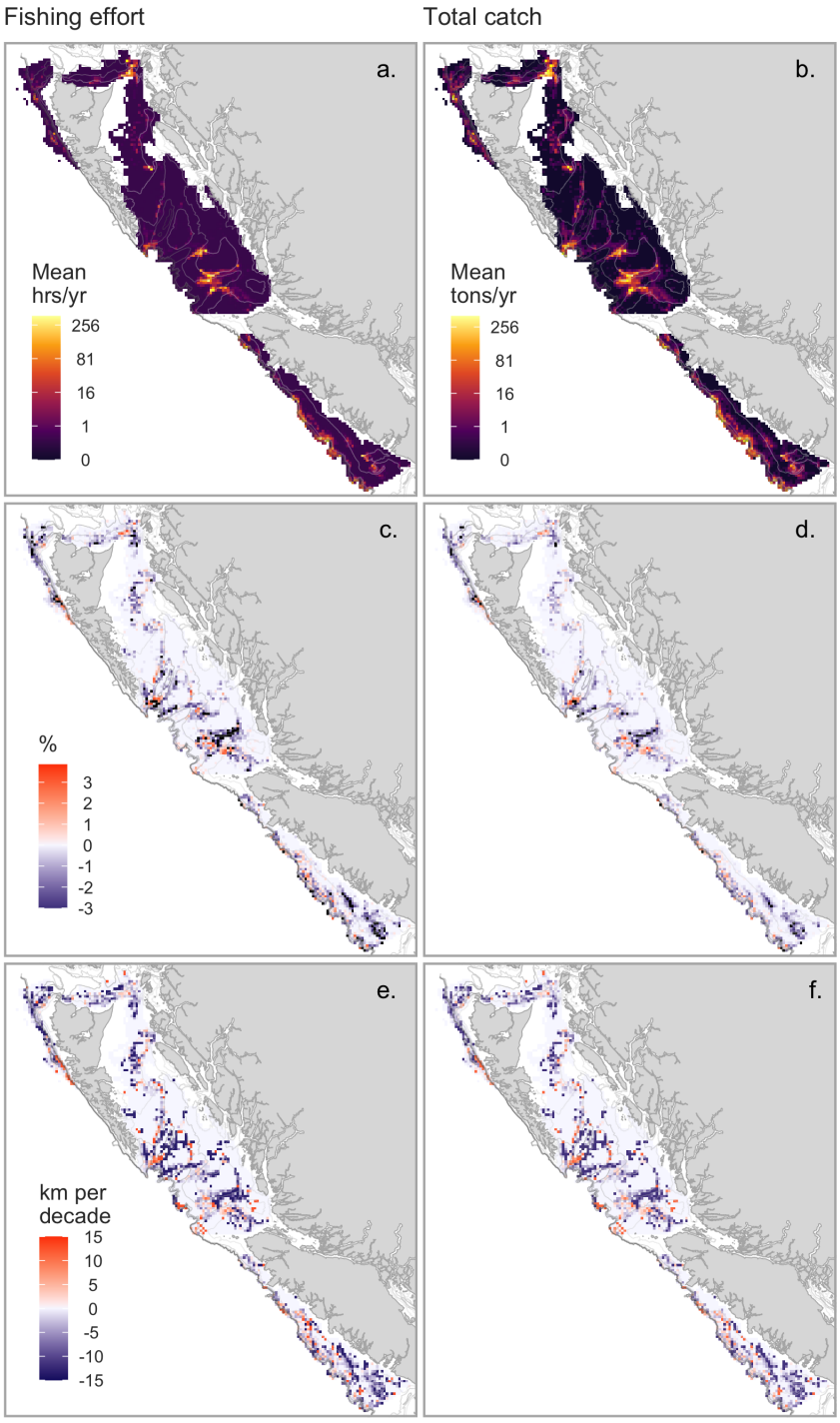

Figure S20: Variables capturing cell-specific commercial trawl fishing intensity: mean hours of commercial trawl fishing conducted (a) and mean tons of fish caught (b) per year, the % change in each estimate of fishing pressure (c, d), and the velocity of change in fishing pressure (e, f) between 2008 and 2018 for each 4×4 km cell within the survey footprint.

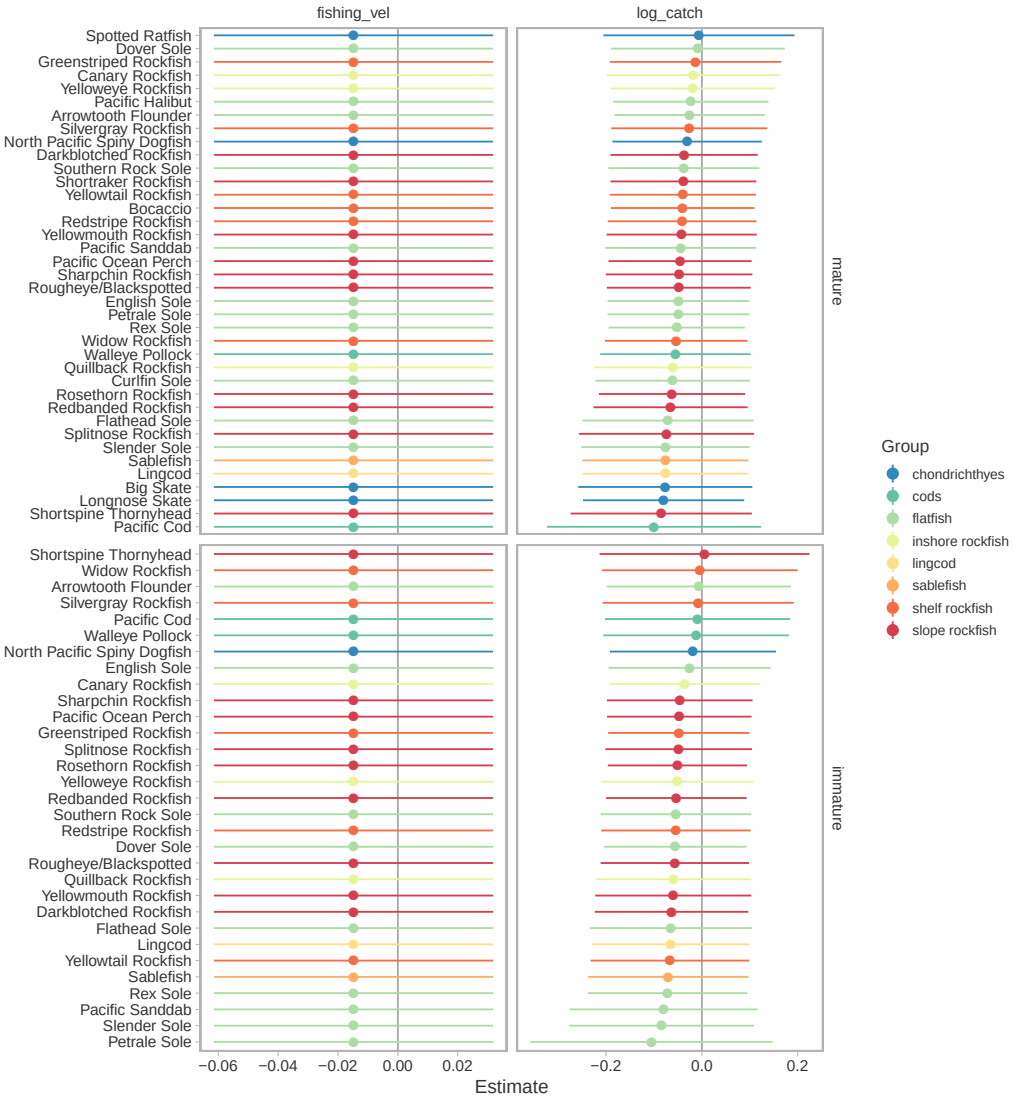

Figure S21: Species-specific coefficient estimates for variables accounting for fishing effort. This model includes the same climate variables as the "Velocity" models in Figures 2b and S22, as well as two variables capturing cell-specific commercial trawl fishing intensity: the velocity of change in mean hours of fishing that occurred annually between 2008 and 2018 (fishing_vel) and the mean tons of fish captured annually across those years (log_catch). Other variables illustrated in Figure S20 were explored, including interactions between mean and change values, but the rest were not estimate-able in models including the full set of climate variables.

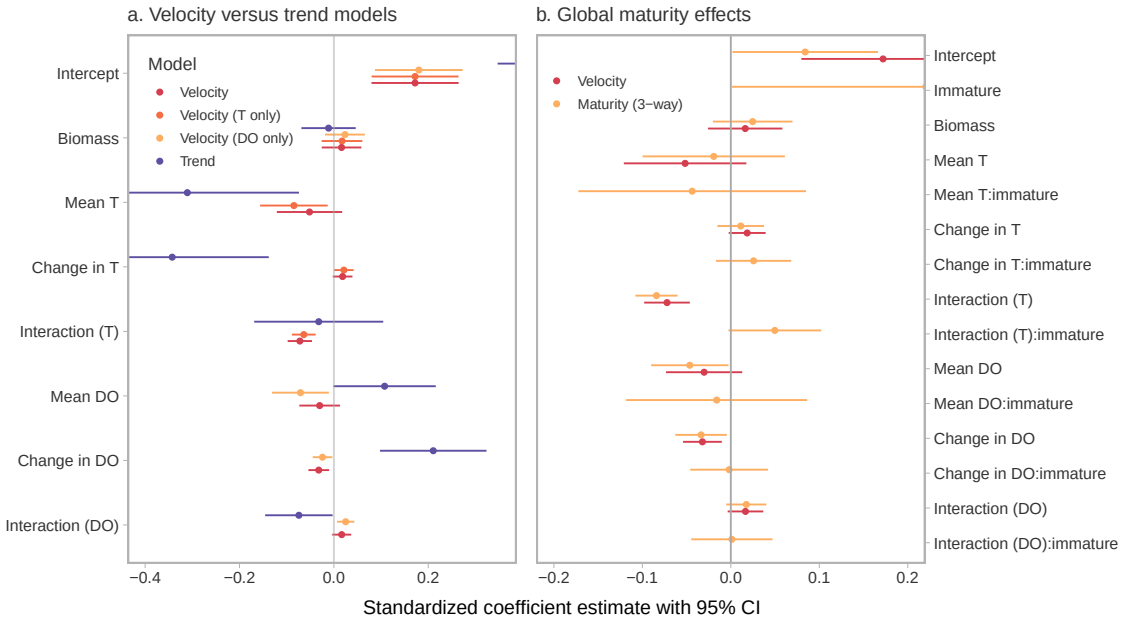

Figure S22: Global coefficient estimates for all fixed effects in a range of model configurations. All 'velocity' models predicted biotic velocity in response to climate changes calculated as gradient-based velocities (trend/spatial gradient). 'Trend' model predicts % change in biomass in response to climate changes measured as trends. Unless noted in parentheses, both temperature (T) and dissolved oxygen (DO) are included in each model. 'Interactions' are between the change in each climate variable (included in parentheses) and the mean conditions for that same climate variable. All models incorporate some degree of density-dependence by including the mean estimated biomass across all years. The model with a maturity effect (b. yellow dot-whisker–climate velocities and means interact with maturity) treats mature populations as the intercept.